Geological Magazine

www.cambridge.org/geo

Original Article

Cite this article: Wu C, Li H, Zheng X, Hong T, Ma Y-C, Xu X-W, Zhang H-J, Wang C-X, and Dong L-H. Petrogenesis and tectonic implications of Hongliutan Precambrian metamorphic rocks in the Tashikuergan-Tianshuihai Terrane, Northwest Tibet, China: insights from geochemical and geochronological studies. *Geological Magazine* **161**(e28): 1–18. https://doi.org/10.1017/S0016756824000360

Received: 24 May 2023
Revised: 24 October 2024
Accepted: 25 October 2024

Keywords:
Metamorphic rocks; geochronological; Precambrian; tectonic evolution; Tibet

Corresponding authors: Xiao Zheng; Email: zxiao@mail.cgs.gov.cn; Hao Li; Email: lihaozky@126.com

Petrogenesis and tectonic implications of Hongliutan Precambrian metamorphic rocks in the Tashikuergan-Tianshuihai Terrane, Northwest Tibet, China: insights from geochemical and geochronological studies

Chu Wu[1], Hao Li[2], Xiao Zheng[1], Tao Hong[3,4], Yin-Ce Ma[2,5], Xing-Wang Xu[2,5], Hui-Jun Zhang[1], Cheng-Xi Wang[1] and Lian-Hui Dong[1,2,6]

[1]Development and Research Center of China Geology Survey, Beijing, PR China; [2]State Key Laboratory of Lithospheric and Environmental Coevolution, Institute of Geology and Geophysics, Chinese Academy of Sciences, Beijing, PR China; [3]Guangdong Provincial Key Lab of Geodynamics and Geohazards, School of Earth Sciences and Engineering, Sun Yat-sen University, Guangzhou, PR China; [4]Southern Marine Science and Engineering Guangdong Laboratory (Zhuhai), Zhuhai, PR China; [5]College of Earth and Planetary Sciences, University of Chinese Academy of Sciences, Beijing, PR China and [6]Xinjiang Bureau of Geology and Mineral Resources, Urumqi, Xinjiang, PR China

Abstract

The Northwest Tibet region is defined by several terranes, magmatic belts, basins and sutures, which were primarily shaped by the tectonic activities associated with Proto-, Palaeo- and Neo-Tethys Oceans. However, the basement nature and Precambrian tectonic evolution of the Northwest Tibet region, particularly within the Tashikuergan-Tianshuihai terrane, remain largely unknown. The Hongliutan area, located in the northeastern part of the Tashikuergan-Tianshuihai terrane, contains a critical sequence of Precambrian metamorphic rock strata. Detailed petrological, geochronological, and geochemical analyses of these metamorphic rocks – including plagioclase schist, quartz schist, amphibolite and nearby leucogranite – reveal the intricate processes of tectonic evolution within the Tianshuihai unit. Combining these findings with previous geochronological results is crucial for re-evaluating the nature of the Tashikuergan-Tianshuihai basement and its Precambrian tectonic evolution of the Tashikuergan-Tianshuihai basement. Our results reveal the following: (1) the leucogranite and amphibolite, identified as Cambrian igneous rocks, display distinct geochemical signatures indicative of a continental arc origin. These include calc-alkaline characteristics, enrichment in Th, U, Pb, Zr and Hf and depletion in Ba, Nb, Sr and Ti. Their $\varepsilon_{Nd}(t)$ values, close to zero, further support this tectonic setting, with the leucogranite and amphibolite formed at 506 and 522 Ma, respectively. (2) The plagioclase schist and quartz schist are interpreted to be Neoproterozoic volcaniclastic rocks that formed in a rifted (passive) continental margin setting. The quartz schist is particularly rich in detrital zircons, displaying a broad spectrum of $^{207}Pb/^{206}Pb$ ages, ranging from 901 to 3364 Ma. (3) A significant subset of detrital zircons within the quartz schist exhibits oscillatory zoning, high Th/U ratios and sharp-edged, anhedral-to-subhedral crystal forms, suggesting a derivation from proximal or deep-seated terranes. The concordant U–Pb zircon ages of 2468 and 974 Ma from the quartz schist, along with the 978 Ma age from the inherited zircons in the amphibolite, and the 1.2–2.1 Ga $T_{2DM}(Nd)$ from leucogranite and metamorphic rocks, collectively suggest that the Tianshuihai unit is likely underpinned by a Palaeoproterozoic basement that indicates Neoproterozoic reworking.

Therefore, our findings suggest the presence of a continuous, northwest-southeast trending Palaeoproterozoic basement underlying the entire Tashikuergan-Tianshuihai terrane. An alternative scenario posits that the ancient basement, currently beneath the Tashikuergan terrane, could extend into the Tianshuihai region, potentially indicating a Cambrian continental margin arc interspersed with remnants of older terranes.

1. Introduction

The Northwest Tibet area, also known as the West Kunlun orogenic belt (Xiao et al., 2002, 2003a, 2003b; Wang et al., 2020), serves as crucial junction between the Central Asia and Tethys tectonic domains (Wang et al., 2016; Zhang et al., 2019a; Yin et al., 2020). The abundant magmatic rocks in this area reveal the evolution of the Proto-, Palaeo- and Neo-Tethys Oceans (Pan, 1996; Xiao et al., 2003a, 2005; Zhang et al., 2019a; Yin et al., 2020). However, limited access and harsh natural conditions have hindered our understanding of the Precambrian magmatic record, and these factors also impeded the study of the basement in the Northwest Tibet area.

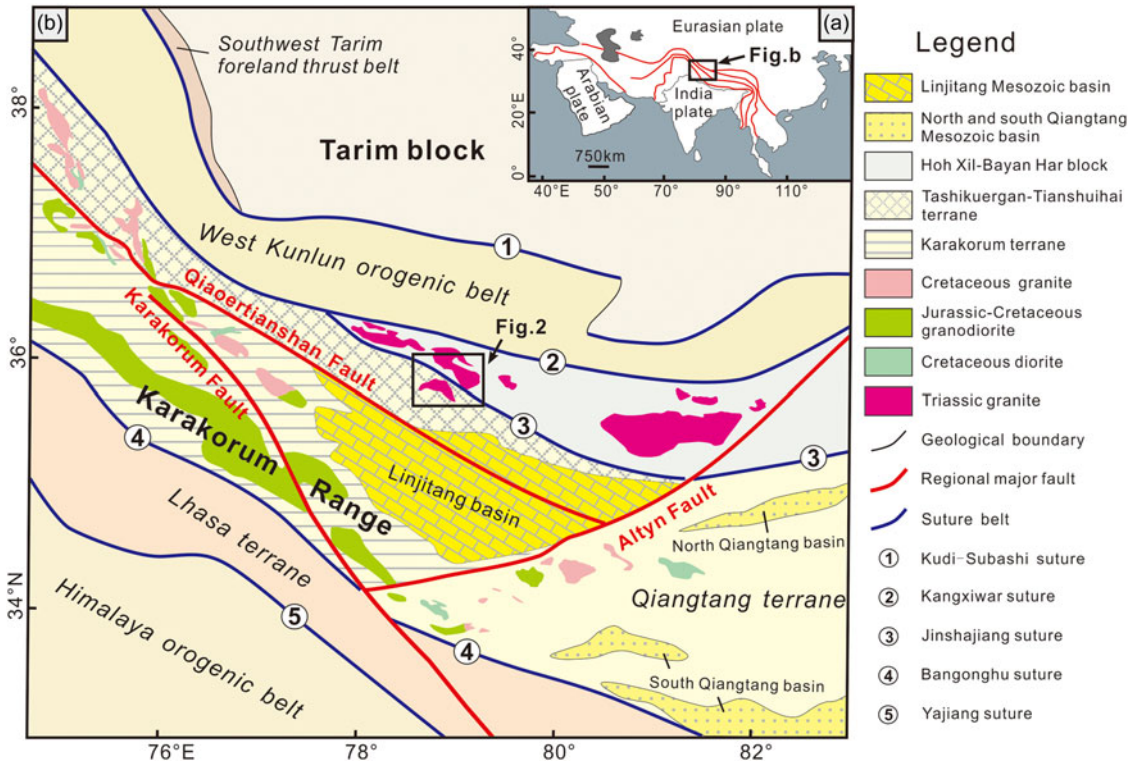

Figure 1. Location (a) and tectonic units (b) of the West Kunlun-Karakorum area (revised from Pan et al., 2004; Li et al., 2009a; Dong et al., 2015; Li et al., 2019).

The Proto-Tethys Ocean is widely believed to have formed by the break-up of the supercontinent Rodinia, spanning from the Neo-Proterozoic until at least the Early Silurian (Ding et al., 1996; Xiao et al., 2003a, 2005; Jia et al., 2013; Wang et al., 2017). Island arc magmatism related to this process may have occurred before the Early Cambrian (>533 Ma; Yin et al., 2020) and continued until the Silurian (Zhang et al., 2018a) in present-day West Kunlun. The later subduction associated with the closure of the Palaeo-Tethys Ocean occurred from the Late Permian to Late Jurassic (Pan, 1996; Matte et al., 1996; Mattern and Schneider, 2000; Xiao et al., 2005; Jiang et al., 2013; Liu et al., 2015). However, the source of the Precambrian to Late Jurassic granitoids remains unclear, and the basement nature and Precambrian tectonic evolution of the Northwest Tibet area, particularly in the Tashikuergan-Tianshuihai terrane, remains largely unknown. Zhang et al. (2020) and Yin et al. (2020) proposed that the Cambrian andesites, dacites and granitoid plutons in the Tashikuergan-Tianshuihai terrane, Northwest Tibet area, were likely derived from partial melting of Palaeo-Proterozoic and Meso-Proterozoic basement rocks. Ji et al. (2011) have reported 2481 ± 14 Ma zircons in foliated rhyolite from the Tashikuergan-Tianshuihai terrane. However, further systematic discussion of their petrogenesis and formation mechanism is still needed to understand the basement nature and tectonic evolution of the Tashikuergan-Tianshuihai terrane. Previous studies have primarily focused on Cambrian to Triassic granitoids (Yuan et al., 2002; Jiang et al., 2002, 2013; Jia et al., 2013; Liu et al., 2015; Zhang et al., 2016, 2019a; Zhang et al., 2020; Yin et al., 2020; Wang et al., 2022), with limited investigation of Precambrian metamorphic igneous and volcaniclastic rocks. These rocks are of critical importance, as they likely represent the magmatic or volcanic products of the assembly and break-up of the supercontinent Rodinia and crucial information about basement formation and evolution. Despite the scarcity of Precambrian metamorphic igneous rocks, their significance warrants further study.

Our recent detailed field investigations in the Hongliutan area, northeastern Tashikuergan-Tianshuihai terrane, have led to the discovery of Precambrian to Early Cambrian metamorphic igneous and volcaniclastic rock strata. In this study, we integrate our field observations with new petrography, geochronology and geochemistry and combine these with previous results to (1) ascertain the source, petrogenesis and formation environment of metamorphic rocks in the Hongliutan area and (2) propose the basement nature and the Precambrian tectonic evolution of the Tashikuergan-Tianshuihai terrane in the Northwest Tibet. These findings have significant implications for delineating the geodynamic evolution of the Proto-Tethys Ocean and Tibetan Plateau.

2. Regional tectonic setting

The Northwest Tibet region is situated between the Tibetan Plateau to the south and the Tarim Basin to the north (Fig. 1a; Hu et al., 2016). It comprises of several tectonic units, including the southwestern Tarim block, West Kunlun orogenic belt, Hoh Xil-Bayan Har block, Tashikuergan-Tianshuihai terrane, Linjitang basin, Karakorum terrane, Qiangtang terrane, Lhasa terrane and Himalaya orogenic belt, arranged from north to south (Fig. 1b; Pan et al., 2004; Li et al., 2009a; Li et al., 2019). These units accreted during the subduction and collision of the Proto- and Palaeo-Tethys Oceans (Mattern and Schneider, 2000; Xiao et al., 2003a, 2003b, 2005; Wang et al., 2020). Our study focuses on the Hongliutan metamorphic igneous rocks in the northeastern part of the Tashikuergan-Tianshuihai terrane. This terrane lies between the West Kunlun orogenic belt, the Hoh Xil-Bayan Har block, the

https://doi.org/10.1017/S0016756824000360

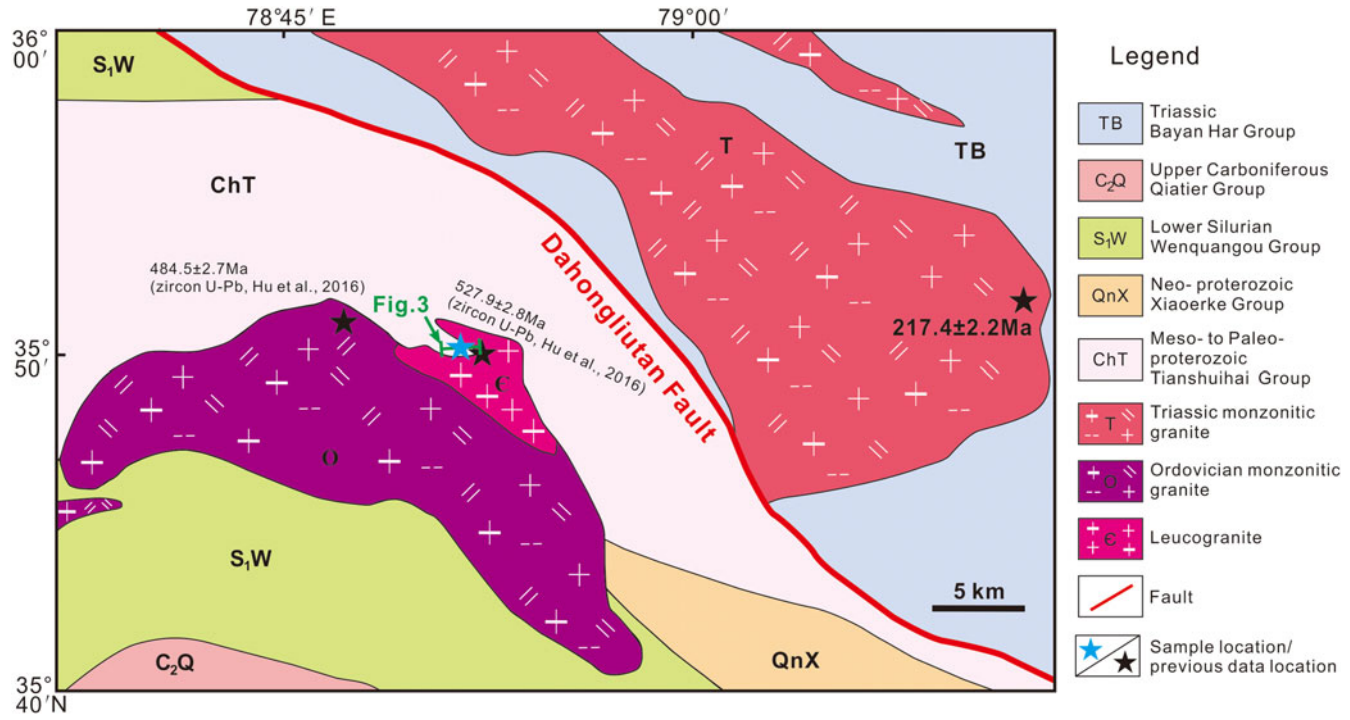

Figure 2. Geological map of the Hongliutan area.

Qiangtang terrane and the Karakorum terrane. The Kangxiwar suture, Jinshajiang suture, Altyn fault and Qiaoertianshan fault separate the Tashikuergan-Tianshuihai terrane from the surrounding units, respectively (Fig. 1b; Pan, 1990; Jiang et al., 1992; Deng, 1995; Yin and Harrison, 2000; Jiang et al., 2002; Chung et al., 2005; Li et al., 2008a; Pan et al., 2012; Li et al., 2019).

The Tashikuergan-Tianshuihai terrane is composed of Precambrian basement and overlying Phanerozoic strata (Wang et al., 2020). The basement consists of a Palaeo-Proterozoic medium- to high-grade metamorphic complex and Meso-Proterozoic metamorphic shallow-marine carbonate rocks, including the Tianshuihai, Bulunkuole and Saitula groups (Ding et al., 1996; Chu, 2008). The terrane cover comprises Palaeozoic strata, including Carboniferous and Permian clastic limestones and other carbonate rocks (Anhui Geological Survey, 2005a, 2005b). A Late Triassic granitoid plutonic belt trends west to east and extends through the Tashikuergan-Tianshuihai terrane and Hoh Xil-Bayan Har block (209.6 Ma and 217.0 to 216.0 Ma; Qiao et al., 2015a; Wei et al., 2017). In the southern part of the terrane, a Jurassic-Cretaceous granodioritic plutonic belt trends southeastward and is situated in the Tashikuergan-Tianshuihai, Karakorum, and Qiangtang terranes (Fig. 1b; Pan et al., 2004, 2012; Li et al., 2008a; Li et al., 2019). The Jurassic-Cretaceous magmatic arc and the Linjitang back-arc basin are related to the northward-directed subduction of the Bangong-Nujiang oceanic plate beneath the Tashikuergan-Tianshuihai and Karakorum terranes (Fig. 1b; Pan et al., 2012; Li et al., 2008a; Li et al., 2019).

3. Geological setting of Hongliutan area

3.a. Lithology

The Tashikuergan-Tianshuihai terrane and Hoh Xil-Bayan Har block are separated by the Dahongliutan fault, which reactivates the western part of the Jinshajiang suture. The Hongliutan area is situated in the northeastern part of the Tashikuergan-Tianshuihai terrane and on the southwestern side of the Dahongliutan fault (Fig. 2). The area is characterized by Meso- to Palaeo-Proterozoic (c.a. 1.4 to 1.8 Ga, Tianshuihai Group), Neo-Proterozoic (ca. 0.8 to 1.0 Ga, Xiaoerke Group), lower Silurian (Wenquangou Group) and upper Carboniferous (Qiatier Group) sediments and metasediments. The Meso- to Palaeo-Proterozoic Tianshuihai Group comprises a suite of greenschist-facies, shallow-marine siliciclastic rocks (e.g. sericite-quartz schist, phyllite, and argillaceous slate), and limestone (Hu et al., 2016; Wang et al., 2020). The Neo-Proterozoic Xiaoerke Group features siliceous dolomite and limestone. The Lower Silurian Wenquangou Group mainly comprises thick layers of grey-green to light-grey feldspar-quartz slate, meta-sandstone and siltstone, interlayered with limestone and marble (Zhang et al., 2019a; Li et al., 2019; Wang et al., 2020).

In addition, an Ordovician monzonitic granitic pluton (484.5 ± 2.7 Ma) and a Cambrian granite porphyry (527.9 ± 2.8 Ma) located to the northeast intruded into the aforementioned sedimentary and metasedimentary sequences (Fig. 2; Qiao et al., 2015b; Hu et al., 2016). The Tashikuergan-Tianshuihai terrane is thought to have been an accretionary prism during the Palaeozoic-Mesozoic and contains thick, partly metamorphosed Triassic flysch sequences that record subduction-related orogenic processes resulting from the collision between the West Kunlun orogenic belt and Karakorum terranes (e.g. Matte et al., 1996; Mattern and Schneider, 2000; Yin and Harrison, 2000; Xiao et al., 2001, 2002, 2003a, 2005; Wang et al., 2020).

3.b. Geological section in the Hongliutan area

A newly discovered metamorphic rock stratum has been found adjacent to the Cambrian leucogranite in the western region. It is exposed along a tightly folded syncline, with both limbs dipping to the northwest and a fold axis plunging to the northeast. This formation measures approximately 3.0 km in length and 0.5 km in width. The eastern part of this syncline exhibits an unconformable

https://doi.org/10.1017/S0016756824000360

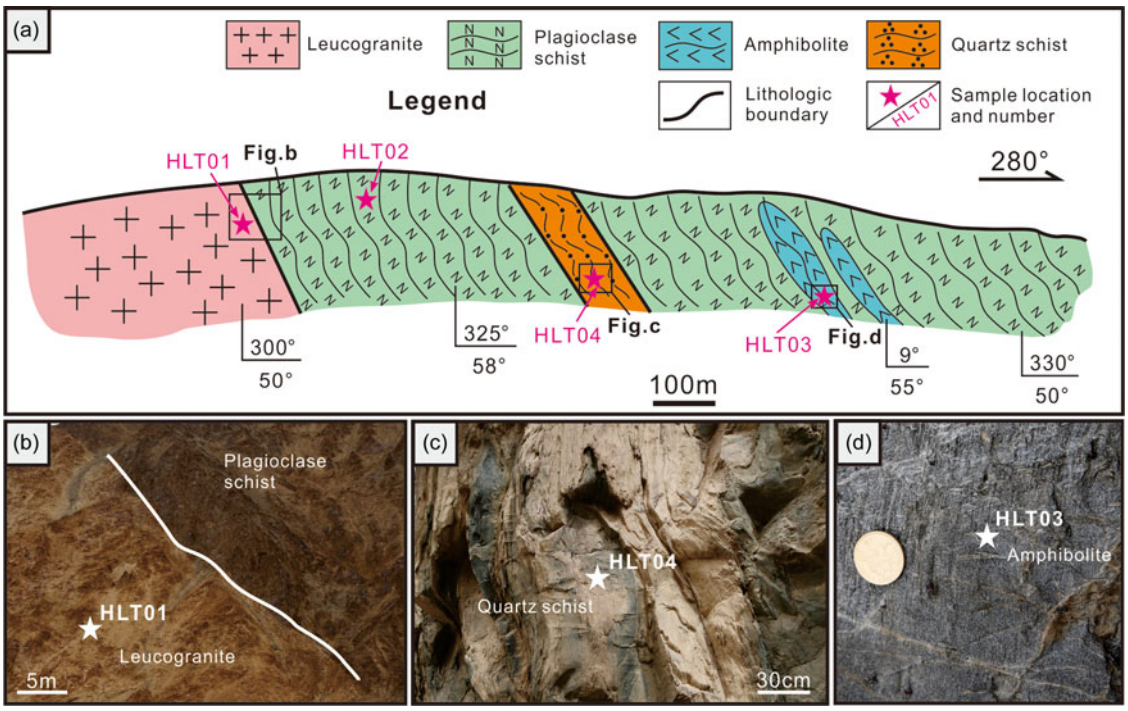

Figure 3. A simplified sketch of the geological section in the Hongliutan area (a). Field photos of leucogranite intrusion into plagioclase schist (b), schistosity in quartz schist (c) and amphibolite layers (d).

contact with the Cambrian leucogranite, with an NW-striking main dip angle of 50° to 60° (Fig. 3a). The stratum is mainly composed of foliated plagioclase schist (Fig. 3b), amphibolite (Fig. 3d), and quartz schist (Fig. 3c). This metamorphic rock stratum was intruded by Cambrian leucogranite and cut by multiple-stage faults (Figs. 3a and 3b). It underwent greenschist-facies to epidote-amphibolite facies metamorphism simultaneously, transforming into middle-low grade metamorphic rocks. The quartz schist, interlayered between layers of plagioclase schist less than 100 m wide, is found alongside intrusive bodies of amphibolite, which are themselves surrounded by the plagioclase schist (Fig. 3a). Detailed stratigraphic descriptions of the granitoid and metamorphic rocks are outlined below:

The leucogranite is a felsic intrusion located to the east of the metamorphic rock stratum (Figs. 3a and 3b). It mainly consists of euhedral to subhedral phenocrysts of 12–20 vol% plagioclase (100–700 μm), 5 vol% quartz (200–500 μm), and 3 vol% muscovite (20–150 μm), as well as an anhedral matrix of felsic minerals (plagioclase and quartz) with minor accessory minerals (apatite, zircon, and ilmenite). The leucogranite exhibits a porphyritic texture (Figs. 4a and 4b).

The grey-dark grey plagioclase schist forms the main body of the metamorphic rock stratum (Figs. 3a and 3b). The foliation is clearly evident with an inclination of 58°, exhibiting a distinct banded structure with oriented minerals under the microscope (Figs. 4c and 4d). The garnet within the plagioclase-quartz-biotite assemblage exhibits a distinct counterclockwise rotation, indicating its original alignment. However, the development of lineation is not obvious. It contains 40 vol% subhedral to anhedral plagioclase (<200 μm) and 35 vol% quartz (<200 μm), euhedral to subhedral 10 vol% biotite (100–250 μm), and 8 vol% chlorite (80–1,200 μm), as well as subhedral 4 vol% garnet (250–500 μm).

The grey quartz schist forms the central part of the metamorphic igneous rock stratum, showing an inclination of 55° (Figs. 3a and 3c), and exhibits a banded structural texture under the microscope (Fig. 4). It mainly comprises subhedral to anhedral fine-grained 50 to 100 μm quartz (35–40 vol%) and plagioclase (30–35 vol%) phenocrysts, oriented euhedral 200 to 600 μm garnet (12–15 vol%), 20 to 500 μm biotite (8–10 vol%), and chlorite (8–10 vol%) phenocrysts (Figs. 4e and 4f). The accessory minerals include apatite, zircon, ilmenite, magnetite, and pyrite.

The grey amphibolites appear as additional intrusions, measuring 200 m in length and 50–80 m in width, within the plagioclase schist section (Figs. 3a and 3d). It mainly comprises subhedral plagioclase (35 vol%, 50–200 μm), quartz (25 vol%, 50–200 μm), biotite (4 vol%, 30–100 μm), and euhedral to subhedral hornblende (35 vol%, 50–700 μm). It is characterized by the curved lineation of hornblende (Figs. 4g and 4h). Therefore, the mineral paragenesis supports an amphibolite facies.

4. Sample selection and analytical techniques

This contribution employed two leucogranite samples (HLT01-2 and HLT01-3), three plagioclase schist samples (HLT02-2, HLT02-3, and HLT02-4), two quartz schist samples (HLT04-3 and HLT04-4), and two amphibolite samples (HLT03-3 and HLT03-4). These samples were selected after detailed petrographic examination as representative samples to evaluate the whole-rock geochemical composition. Major and trace element abundances were obtained by using X-ray fluorescence (XRF) spectrometry and inductively coupled plasma mass spectrometry (ICP-MS), respectively. The detailed preparation and analysis process were described in Hong et al. (2018) and Wu et al. (2018). The international standard samples, GSR-1 (granite) and GSR-3 (basalt), were used to monitor the preparation process and instrument status. Analytical uncertainties were 1–3% for major elements, 5% for rare earth elements (REEs), and 5–10% for trace

https://doi.org/10.1017/S0016756824000360

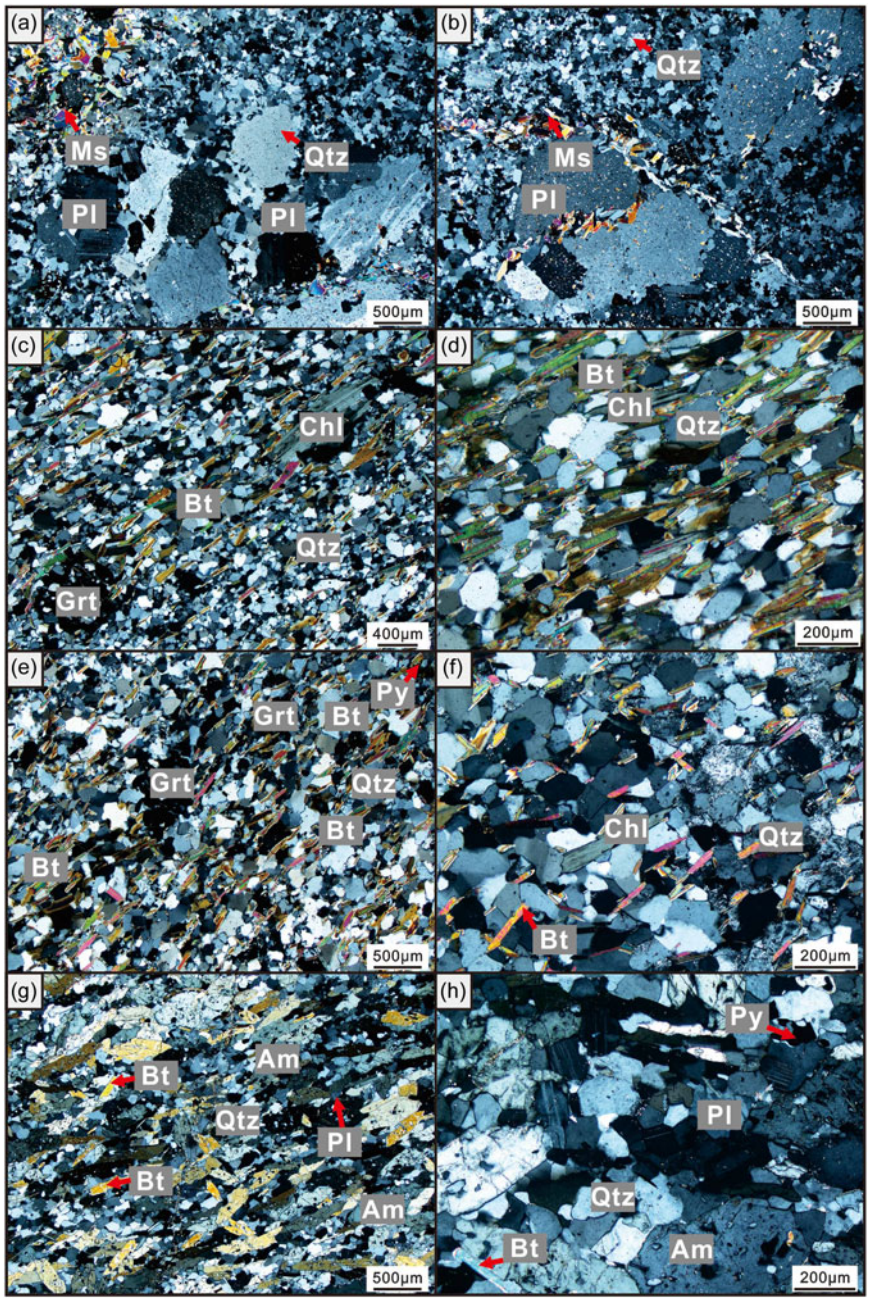

Figure 4. Photomicrographs of leucogranite (a, b), plagioclase schist (c, d), quartz schist (e, f) and amphibolite (g, h). Abbreviations: Am–amphibole, Bt–biotite, Chl–chlorite, Grt–garnet, Ms–muscovite, Pl–plagioclase, Py–pyrite, and Qtz–quartz.

elements. The whole-rock major and trace element data are listed in Supplementary Table DR1.

To evaluate the Rb–Sr and Sm–Nd isotopic compositions, we employed the leucogranite samples HLT01-2 and HLT01-3, plagioclase schist sample HLT02-2, quartz schist sample HLT04-3, and amphibolite sample HLT03-3, all corresponding to the bulk rock samples. Sr–Nd isotope analyses were performed by using the classical two-step ion-exchange chromatographic method and measured using a Thermo Fisher Triton Plus multi-collector thermal ionization mass spectrometer. The Sr and Nd isotopic ratios were respectively normalized to $^{86}Sr/^{88}Sr = 8.375209$ and $^{146}Nd/^{144}Nd = 0.7219$. During the data acquisition period, Sr standard NBS-987 gave $^{87}Sr/^{86}Sr = 0.710265 \pm 0.000014$ ($n = 4$, 2σ), and JNdi-1 Nd standard yielded $^{143}Nd/^{144}Nd = 0.512110 \pm 0.000009$ ($n = 4$, 2σ). Additionally, the leucogranite samples HLT01-2 and HLT01-3, plagioclase schist samples HLT02-2 and HLT02-3, quartz schist samples HLT04-3 and HLT04-4, and amphibolite samples HLT03-3 and HLT03-4 were analysed for Pb isotope analyses. Pb was separated and purified using the conventional cation-exchange technique, yielding procedural blanks with Pb concentrations of 200 pg. Repeated analysis of the NBS981 gave a value of $^{207}Pb/^{206}Pb = 0.91405 \pm 0.00040$ (2σ). The detailed preparation and analysis process for the above Sr–Nd–Pb isotopic tests followed procedures similar to those described by Li et al. (2015, 2016). The results of the Sr–Nd–Pb isotopic analysis are summarized in Supplementary Table DR1.

Zircon grains from part of the samples were collected for U–Pb dating using laser ablation (LA) ICP-MS (sample HLT01-1, leucogranite, 14 grains) and secondary ion mass spectrometry

https://doi.org/10.1017/S0016756824000360

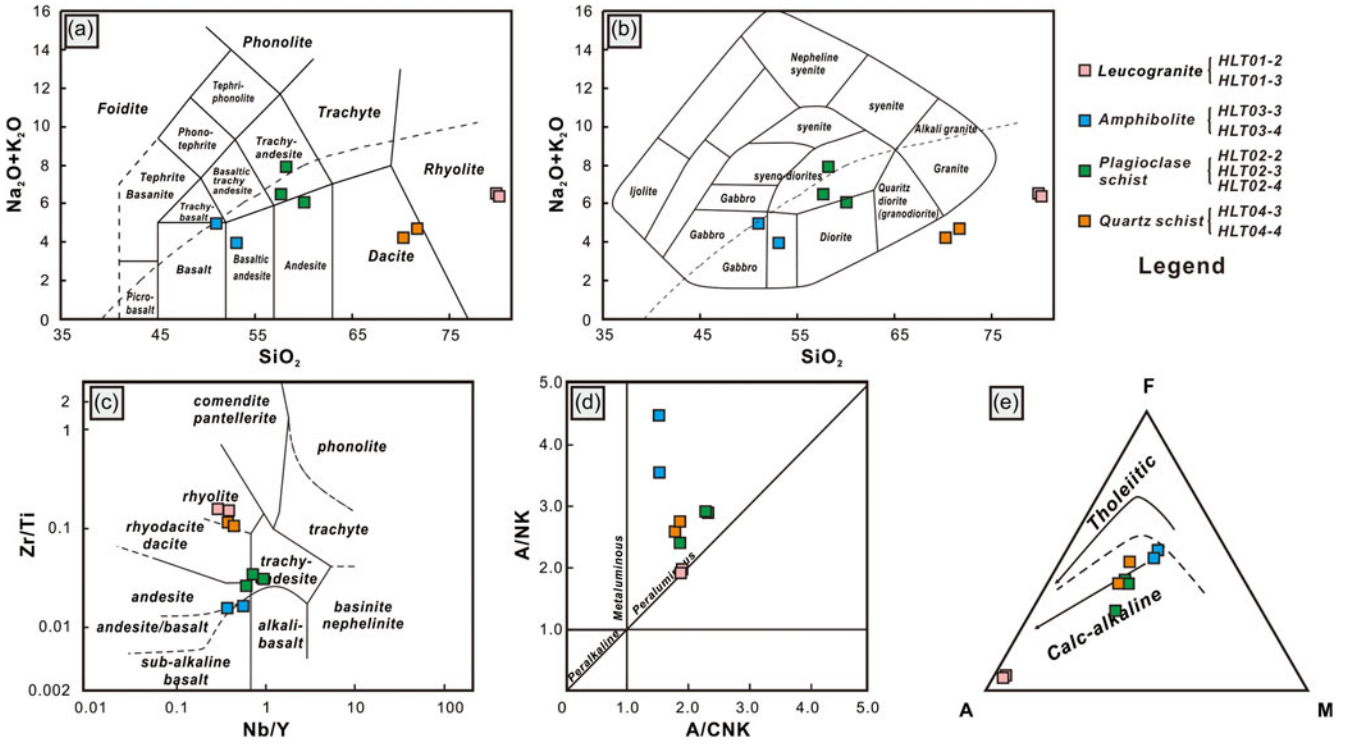

Figure 5. Geochemical diagrams for Hongliutan leucogranite and metamorphic rocks: (a, b) The TAS diagram (after Le Bas et al., 1986; Wilson, 1989), (c) Nb/Y versus Zr/Ti diagram (after, Winchester and Floyd, 1977), (d) A/CNK versus A/NK diagram (after Maniar and Piccoli, 1989) and (e) AFM diagram (after Irvine and Baragar, 1971).

(SIMS) (sample HLT04-2, quartz schist, 43 grains; sample HLT03-2, amphibolite, 14 grains). Conventional heavy fraction and magnetic techniques were used for sample separation. The freshest, unbroken, and representative zircon grains were selected and mounted in epoxy mounts. The morphology, internal structure, pellucidity, inclusions, and zonation were revealed in transmitted and reflected light photomicrographs and cathodoluminescence (CL) images. All epoxy mounts were polished to expose half-sections of the zircon grains and vacuum-coated with high-purity gold before CL imaging and LA-ICP-MS/SIMS analysis. Measurements of U, Th, and Pb were conducted using the Agilent 7500a Q-ICP-MS with a 193 nm excimer laser ablation system and the Cameca IMS-1280 SIMS. LA-ICP-MS followed operating and data processing procedures similar to those described by Xie et al. (2008), and a detailed description of the Cameca IMS-1280 SIMS analytical procedure is given in Li et al. (2009b). Common-Pb corrections and data reductions were made using the method of Andersen (2002) and the Isoplot/Ex version 2.49 programs of Ludwig (2001). Errors quoted as age dates are at the 2σ level. All zircon U–Pb data is presented in Supplementary Tables DR2 and DR3.

All of the above analyses were conducted at the Institute of Geology and Geophysics, Chinese Academy of Sciences (IGGCAS), China.

5. Results

5.a. Major and trace element compositions

The analysed samples have low loss on ignition (LOI) values ranging from 0.48 wt% to 2.16 wt%, with no observed positive relationship between LOI and K_2O or $K_2O + Na_2O$. The leucogranite and amphibolite are classified as igneous rocks. Accordingly, we utilize geochemical diagrams specifically designed for igneous rocks to identify their distinct types and characteristics. While the geochemical data for the plagioclase schist and quartz schist strongly suggest a volcaniclastic origin, it is important to note that other origins cannot be entirely ruled out, as the geochemical evidence remains insufficient. Therefore, geochemical diagrams typically used for sedimentary rocks were applied to assess their characteristics, while also considering igneous rock diagrams for comparison.

These samples exhibit a wide compositional variation, with SiO_2 contents varying from 51.04 to 80.23 wt% and Zr/Ti ratios from 0.02 to 0.16, ranging from basalt (gabbro) to rhyolite (granite) compositions (Figs. 5a–c; Le Bas et al., 1986; Wilson, 1989; Winchester and Floyd, 1977). All samples are peraluminous and belong to the calc-alkaline series, as shown in the A/CNK versus A/NK (Fig. 5d; Maniar and Piccoli, 1989) and AFM (Fig. 5e; Irvine and Baragar, 1971) diagrams, respectively.

The leucogranite samples (HLT01-2 and HLT01-3) exhibit relatively high SiO_2 contents (79.92 wt% and 80.23 wt%) and Na_2O (5.73 wt% and 5.45 wt%) contents, along with high Zr/Ti ratios of 0.16 and 0.15. These samples are plotted in the rhyolite field of the TAS diagram (Fig. 5a; Le Bas et al., 1986) and the Nb/Y versus Zr/Ti diagram (Fig. 5c; Winchester and Floyd, 1977), and near the granite field in the TAS diagram for plutonic rocks (Fig. 5b; Wilson, 1989). These leucogranite samples are enriched in LREE (LREE/HREE ratios of 5.38 and 6.00, $(La/Yb)_N$ of 5.42 and 5.93) and exhibit flat HREE, and show significant negative Eu anomalies (Eu/Eu* ratios of 0.07 and 0.08; Fig. 6a; Boynton, 1984). In the primitive mantle-normalized diagrams, they exhibit relative enrichments in Rb, Th, Nd, Zr, and Hf, and depletions of Ba, Nb, Sr, P, Eu, and Ti (Fig. 6b; Sun and McDonough, 1989).

The amphibolite samples (HLT03-3 and HLT03-4) exhibit relatively low contents of SiO_2 (51.04 wt% and 53.13 wt%), with high contents of TFe_2O_3 (10.91 wt% and 10.36 wt%), MnO (0.11 wt

https://doi.org/10.1017/S0016756824000360

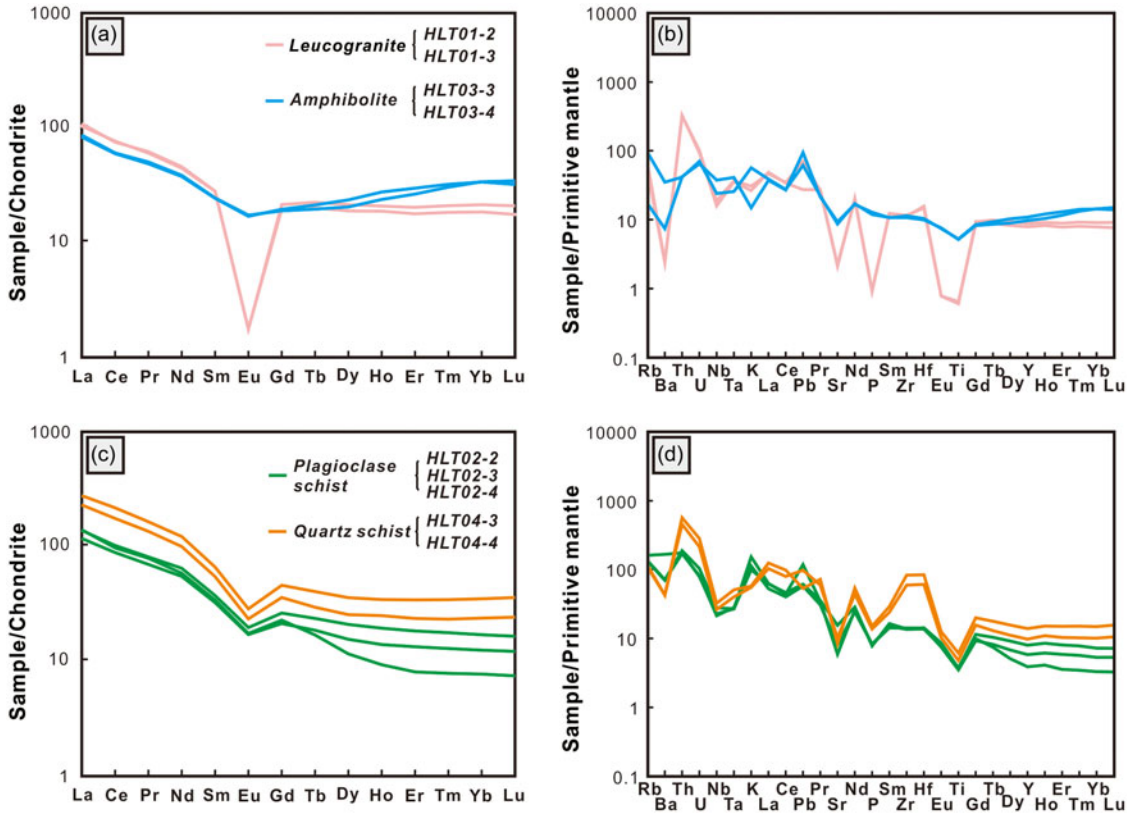

Figure 6. (a, c) Chondrite-normalized REE patterns (after Boynton, 1984) and (b, d) primary mantle-normalized incompatible trace element patterns of the Hongliutan leucogranite and metamorphic rocks (after Sun and McDonough, 1989).

% and 0.13 wt%), MgO (5.83 wt% and 5.16 wt%), and CaO (6.49 wt % and 7.56 wt%). These samples plot within the basaltic andesite, trachybasalt, and gabbro fields of the two TAS diagrams (Figs. 5a and 5b; Le Bas et al., 1986; Wilson, 1989) and in the basalt and sub-alkaline basalt fields of the Nb/Y versus Zr/Ti diagram (Fig. 5c; Winchester and Floyd, 1977). The REE are weakly fractionated, with relatively low LREE/HREE ratios (3.84 and 3.49) and $(La/Yb)_N$ of 2.71 and 2.62, accompanied by negative Eu anomalies (Fig. 6a; Boynton, 1984). These samples exhibit relative enrichments in Rb, U, Pb, and Nd, as well as depletions of Ba, Sr, and Ti on primitive mantle-normalized diagrams, along with variable depletions of K (Fig. 6b; Sun and McDonough, 1989).

The plagioclase schist samples (HLT02-2, HLT02-3, and HLT02-4) exhibit elevated levels of Al_2O_3 (17.61 to 18.93 wt%) and K_2O (3.02 to 4.65 wt%). In the Rb versus K_2O diagram (Fig. 7a; Shen et al., 2009), these samples plot in the felsic domain, and in the ΣREE versus La/Yb diagram (Fig. 7b; Liu, 1991), they are classified within the granite field. In igneous rock geochemical discrimination diagrams, these samples plot in the trachy-andesite and andesite regions on the TAS diagram (Fig. 5a; Le Bas et al., 1986), and in the Nb/Y versus Zr/Ti diagram (Fig. 5b; Winchester and Floyd, 1977). They also plot the syeno-diorite and diorite regions in the TAS diagram for plutonic rocks (Fig. 5b; Wilson, 1989). Total REE concentrations vary from 176.50 to 208.20 ppm with enrichment in LREE (LREE/HREE ratios from 7.42 to 11.68, $(La/Yb)_N$ from 8.62 to 19.19) (Fig. 6c; Boynton, 1984). They are enriched in Rb, Th, K, Pb, Nd, Zr, and Hf, but depleted in Nb, Ta, La, Ce, Sr, P, and Ti on primitive mantle-normalized diagrams (Fig. 6d; Sun and McDonough, 1989).

The quartz schist samples, HLT04-3 and HLT04-4, exhibit relatively high SiO_2 contents (70.34 wt% and 71.77 wt%) and relatively low Al_2O_3 contents (11.62 wt% and 12.16 wt%), respectively. Their plots are located in the felsic domain and granite domain on the Rb versus K_2O diagram (Fig. 7a; Shen et al., 2009) and the ΣREE versus La/Yb diagram (Fig. 7b; Liu, 1991), respectively. In the two TAS diagrams, they respectively plot within the dacite field and near the quartz diorite (granodiorite) field (Figs. 5a and 5b; Le Bas et al., 1986; Wilson, 1989). The samples show total REE concentrations of 335.54 ppm and 416.07 ppm and are characterized by enrichment in LREE, with $(La/Yb)_N$ of 8.42 and 10.29 (Fig. 6c; Boynton, 1984). In primitive mantle-normalized diagrams, the trace element concentrations show depletion in Ba, Nb, Sr, P, Eu, and Ti, and enrichment in Rb, Th, U, La, Ce, Nd, Zr, and Hf (Fig. 6d; Sun and McDonough, 1989).

5.b. Sr–Nd–Pb isotopes

The leucogranite samples (HLT01-2 and HLT01-3) exhibit $(^{87}Sr/^{86}Sr)_i$ ratios of 0.719779 and 0.721624, $(^{143}Nd/^{144}Nd)_i$ ratios of 0.512013 and 0.512026, $\varepsilon_{Nd}(t)$ values of +0.4 and +0.6, $T_{DM}(Nd)$ ages of 1245 Ma and 1181 Ma, and $T_{2DM}(Nd)$ ages of 1197 Ma and 1176 Ma. The amphibolite sample (HLT03-3) exhibits $(^{87}Sr/^{86}Sr)_i$, (143Nd/144Nd)i, $\varepsilon_{Nd}(t)$ values, $T_{DM}(Nd)$ age, and $T_{2DM}(Nd)$ age of 0.715405, 0.511964, −0.6, 1329 Ma, and 1275 Ma, respectively.

The plagioclase schist sample (HLT02-2) has a mean $(^{87}Sr/^{86}Sr)_i$ ratio of 0.723142, $(^{143}Nd/^{144}Nd)_i$ ratio of 0.511418, $\varepsilon_{Nd}(t)$ value of −11.3, $T_{DM}(Nd)$ age of 2120 Ma, and $T_{2DM}(Nd)$ age of 2139 Ma.

https://doi.org/10.1017/S0016756824000360

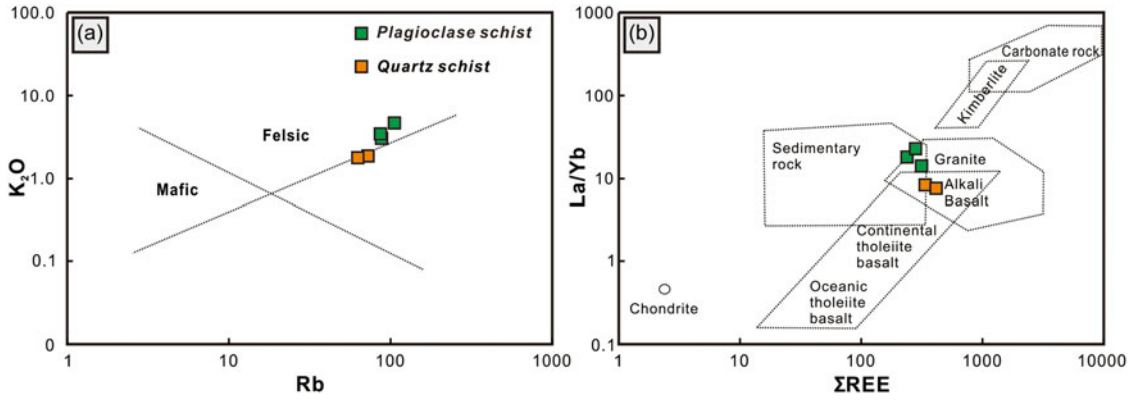

Figure 7. (a) The Rb versus K_2O diagram (after Shen et al., 2009) and (b) the ΣREE versus La/Yb diagram (after Liu, 1991) of the Hongliutan plagioclase schist and quartz schist.

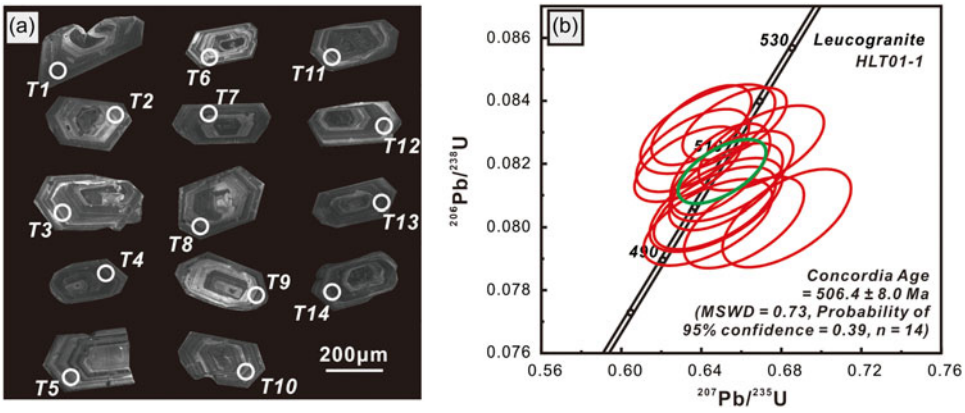

Figure 8. (a) The CL photo and (b) LA-ICP-MS U–Pb concordia age diagram of zircons of the Hongliutan leucogranite. The solid ellipses in the CL photo represent the analytical location of U–Pb age. The numbers adjacent to the solid ellipses show the plot number (n).

The quartz schist sample (HLT04-3) shows $(^{87}Sr/^{86}Sr)_i$ value of 0.714030, $(^{143}Nd/^{144}Nd)_i$ value of 0.511073, $\varepsilon_{Nd}(t)$ value of −6.0, $T_{DM}(Nd)$ age of 1741 Ma, and $T_{2DM}(Nd)$ age of 2115 Ma.

All samples show relatively high $^{208}Pb/^{204}Pb$ ratios ranging from 39.858 to 44.339, $^{207}Pb/^{204}Pb$ ratios ranging from 15.805 to 16.056, and $^{206}Pb/^{204}Pb$ ratios ranging from 19.237 to 22.951 (Supplementary Table DR1).

5.c. Geochronology

Zircons from the leucogranite sample (HLT01-1) and amphibolite sample (HLT03-2) display distinct oval (or sectored) cores and oscillatory zoning in CL images (Figs. 8a and 9a). They also show elevated Th/U ratios ranging from 0.04 to 1.17 with nearly 97% of measurements above 0.1 (Belousova et al., 2002; Long et al., 2007, Supplementary Tables DR2 and DR3), similar to magmatic or regrowth magmatic zircons. Some zircons appear to be inherited from earlier zircon grains, which are mantled by zircon overgrowths and/or present absorption borders (Figs. 9a and 10a, e.g. Hong et al., 2017; Wu et al., 2023). Additionally, they are not detrital zircons, despite being obtained from amphibolite. One common feature of magmatic zircon is its tetragonal shape, typically forming as doubly-terminated prismatic crystals (Corfu et al., 2003). In contrast, detrital zircon is characterized by high grain roundness in morphology (e.g. Pietranik et al., 2008; Rojas-Agramonte et al., 2011). Another typical feature of magmatic zircon is well-developed growth zoning (Corfu et al., 2003). This feature is most evident in CL images, but in detrital zircon affected by physical and chemical processes, variations and disruption in zoning become apparent under microscopic examination. Therefore, the core and oscillatory zoning were chosen as the target areas for LA-ICP-MS and SIMS analyses, respectively, in this study.

Fourteen zircons from the leucogranite sample (HLT01-1) exhibit euhedral morphology with clear zoning, ranging in length from 200 to 300 μm and have elongation ratios from 2 to 4 (Fig. 8a). The LA-ICP-MS analytical plots yield a concordia age of 506.4 ± 8.0 Ma (MSWD = 0.73), with $^{206}Pb/^{238}U$ ages ranging from 496.9 ± 11.4 Ma to 515.6 ± 9.0 Ma, and Th/U ratios from 0.27 to 0.44 (Fig. 8b).

Zircons from the amphibolite sample (HLT03-2) vary in size from 50 to 120 μm with elongation ratios from 1 to 3 (Fig. 9a). These zircons can be divided into three groups (Fig. 9b). Group 1 zircons (7 grains of zircons) display clear oscillatory zoning and have Th/U ratios ranging from 0.40 to 1.17, which are greater than 0.4 as reported by Belousova et al. (2002), and are typical of magmatic zircons. Their plots yield a concordia age of 521.8 ± 9.4 Ma (MSWD = 0.18), with $^{206}Pb/^{238}U$ ages ranging from 507.3 ± 14.6 Ma to 530.8 ± 15.4 Ma, clearly indicating the emplacement time of the amphibolite (Fig. 9c). Group 2 and Group 3 zircons are inherited zircons with ellipsoid morphology and obvious absorption borders. The four zircons from Group 2 have Th/U ratios of 0.36 to 0.68 and yield a concordia age of 977.9 ± 28.0 Ma (MSWD = 1.60) (Fig. 9c). This age may represent the basement age or reflect a large-scale tectonic-magmatic activity. The four inherited zircons in Group 3, which are grains 2, 5, 6, and 7,

https://doi.org/10.1017/S0016756824000360

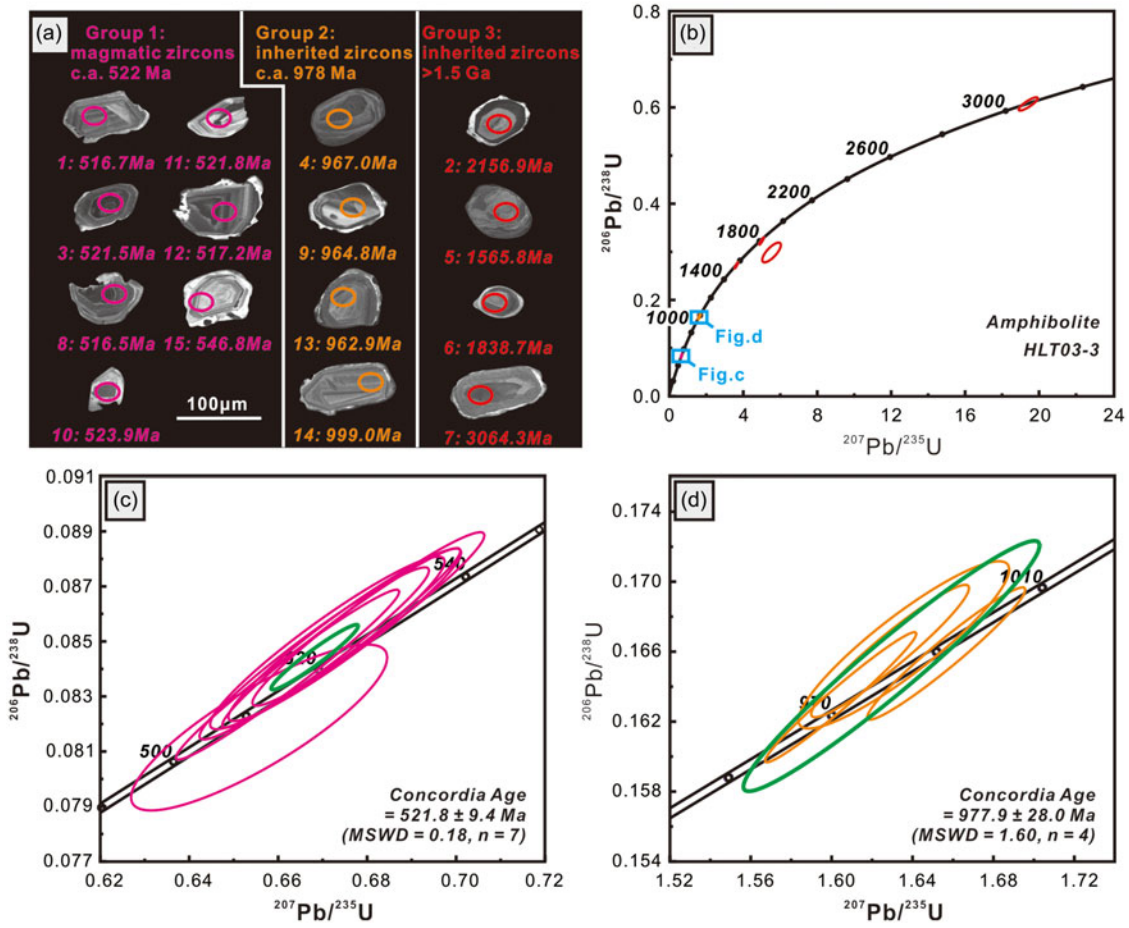

Figure 9. (a) The CL photo and (b-d) SIMS U–Pb concordia age diagrams of zircons of the Hongliutan amphibolite. The solid ellipses in the CL photo represent the analytical location of U–Pb age. The numbers adjacent to the solid ellipses show the plot number (n) with $^{207}Pb/^{206}Pb$ age data.

have ages over 1.5 Ga, with $^{207}Pb/^{206}Pb$ ages ranging from 1566 ± 22.8 Ma to 3064 ± 29.0 Ma.

The CL images reveal that the majority of detrital zircons from the quartz schist sample (HLT04-2) are characterized by sharp-edged anhedral-to-subhedral crystals with distinct concentric oscillatory zoning (Fig. 10a). Their elevated Th/U ratios, with nearly 91% of the measurements exceeding 0.1 (Belousova et al., 2002; Long et al., 2007, Supplementary Table DR3), suggest a proximal igneous source for the zircons. A subset of ancient detrital zircons displays low luminescence and nebulous zoning (Fig. 10a), but their high Th/U ratios are also indicative of an igneous derivation (Hanchar and Rudnick, 1995). Additionally, some detrital zircons possess low luminescent rims with diminished Th/U ratios falling below 0.1 (as seen in Plots 18, 24, 39, and 40, Supplementary Table DR3), lacking the oscillatory zoning typical of the core. These rims are interpreted as evidence of metamorphic overgrowths (Corfu et al., 2003; Long et al., 2007).

The quartz schist sample (HLT04-2) contains four groups of detrital zircons, each characterized by distinct features and age ranges. The zircons exhibit $^{207}Pb/^{206}Pb$ ages ranging from 901 ± 16.8 Ma to 3364 ± 12.8 Ma and yield a discordant line with a lower and upper intercept age of 1003 Ma and 2480 Ma, respectively (Fig. 10b). The Group 1 comprises zircons with magmatic characteristics, including low roundness with sharp edges, clear oscillatory zoning, and relatively high Th/U ratios ranging from 0.11 to 0.85. These features yield a concordia age of 973.7 ± 6.2 Ma (MSWD = 0.56) (Fig. 10c). The Group 2 contains three detrital zircons with a spherical morphology and unsharp corrosion rims, yielding $^{207}Pb/^{206}Pb$ ages from 1597 ± 12.4 Ma to 2082 ± 6.0 Ma. The Group 3 comprises seventeen zircons with $^{207}Pb/^{206}Pb$ ages ranging from 2423 ± 22.6 Ma to 2528 ± 13.6 Ma. Ten zircons in the Group 3 zircons have Th/U ratios ranging from 0.04 to 0.99, and yield a concordia age of 2468.1 ± 22.0 Ma (MSWD = 7) (Fig. 10d), potentially reflecting a Palaeoproterozoic source. The Group 4, previously described, includes eleven detrital zircons that indicate even older $^{207}Pb/^{206}Pb$ ages, ranging from 2609 ± 11.0 Ma to 3364 ± 12.8 Ma.

6. Discussion

6.a. The protoliths of plagioclase schist, quartz schist, and amphibolite

The plagioclase schist and quartz schist in the Hongliutan area are characterized by their foliated mineral assemblages. These rocks have undergone metamorphism ranging from greenschist-facies to amphibolite facies, resulting in the transformation of micas, albite, and chlorite (Figs. 4c and 4d). Additionally, the rotation and recrystallization of rounded plagioclase and quartz subgrains, coupled with garnet overgrowth on biotite and quartz, provide evidence that the interior sections of these rocks have experienced deformation under ductile conditions (Figs. 4e and 4f). The

https://doi.org/10.1017/S0016756824000360

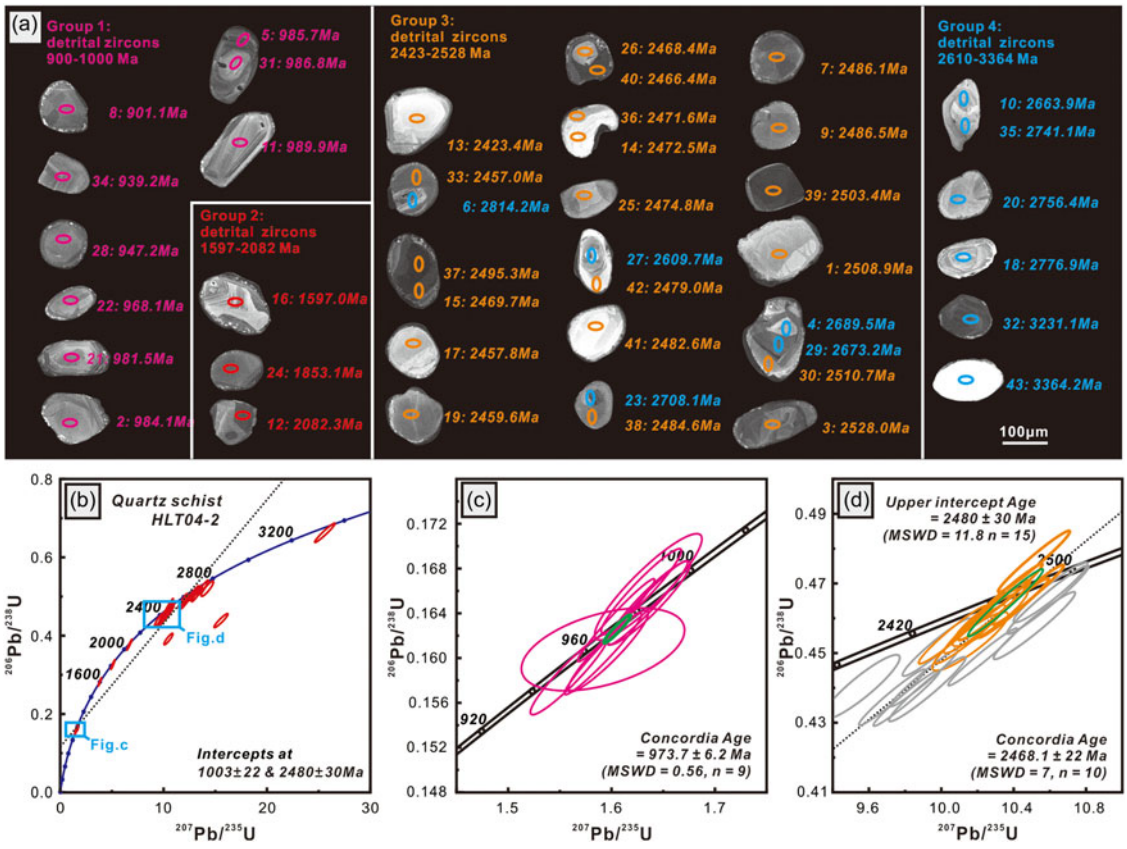

Figure 10. (a) The CL photo and (b-d) SIMS U–Pb concordia age diagrams of zircons of the Hongliutan quartz schist. The solid ellipses in the CL photo represent the analytical location of U–Pb age. The numbers adjacent to the solid ellipses show the plot number (n) with $^{207}Pb/^{206}Pb$ age data.

interlayered contact observed between the plagioclase schist and quartz schist (Figs. 3a and 3c), along with their similar mineral compositions, structural deformation, and alteration patterns, suggests that the protoliths of these rocks are contemporaneous volcaniclastic rocks.

The protoliths of the plagioclase schist and quartz schist are inferred to be andesitic tuff and dacitic tuff, respectively. Geochemical analysis places their plots within the felsic domain and granite domain on the Rb versus K_2O diagram and the ΣREE versus La/Yb diagram (Fig. 7a and 7b; Shen et al., 2009; Liu, 1991), indicating an acidic magmatic source. Detrital zircons from the quartz schist samples display features consistent with a magmatic source, including oscillatory zoning, high Th/U ratios, and sharp-edged anhedral-to-subhedral morphologies (Fig. 10a). These features, combined with their limited transportation, suggest a proximal igneous source. Additionally, the geochemical signatures of these rocks align with those commonly observed in intermediate acid igneous rocks, further supporting an igneous origin (Figs. 5a-e) (e.g. Winter and John, 2001; Le Bas et al., 1986; Wilson, 1989; Winchester and Floyd, 1977; Maniar and Piccoli, 1989; Irvine and Baragar 1971).

The lance-shaped amphibole and biotite within the amphibolite exhibit weak epidotization and chloritization, suggesting a metamorphic progression from greenschist-facies to epidote-amphibolite facies conditions (Figs. 4g and 4h). Geochemical analysis of the amphibolite samples indicates a relatively low SiO_2 content, with values of 51.04 wt% and 53.13 wt%, consistent with the geochemical signatures of pyroxene diorite or gabbro (Figs. 5a-c; Le Bas et al., 1986; Wilson, 1989; Winchester and Floyd, 1977). Combined with the relationship between amphibolite and plagioclase schist (Fig. 3), these findings collectively suggest that the amphibolite represents a mafic intrusive phase that was emplaced after the formation of the volcaniclastic rocks.

The juxtaposition of mafic amphibolite with more felsic volcaniclastic rocks provides significant insights into the magmatic and metamorphic processes of the region. Petrogeochemistry analysis, with its capacity to clearly and intuitively reveal the petrogenesis of both volcaniclastic and igneous rocks, serves as an indispensable tool in deciphering the complex geological history of the area (e.g. Xu et al., 2015a, 2015b; Wu et al., 2020).

6.b. The tectonic setting for the formation of leucogranite and metamorphic rocks

Previous studies on the ca. 500–530 Ma rock association, including mafic and intermediate-acidic volcanogenic sediments and leucogranite, suggested that the Tianshuihai unit likely represents a Cambrian continental margin arc, associated with the southward subduction of the Proto-Tethys Ocean (Hu et al., 2017; Wang et al., 2017; Zhang et al., 2018a, 2018b, 2019b). In this study, the leucogranite, amphibolite, plagioclase schist, and quartz schist exhibit continental arc geochemical characteristics, as supported by the following evidence:

(1) All analysed samples display a calc-alkaline affinity with no indication of tholeiitic rocks, which are typically associated

https://doi.org/10.1017/S0016756824000360

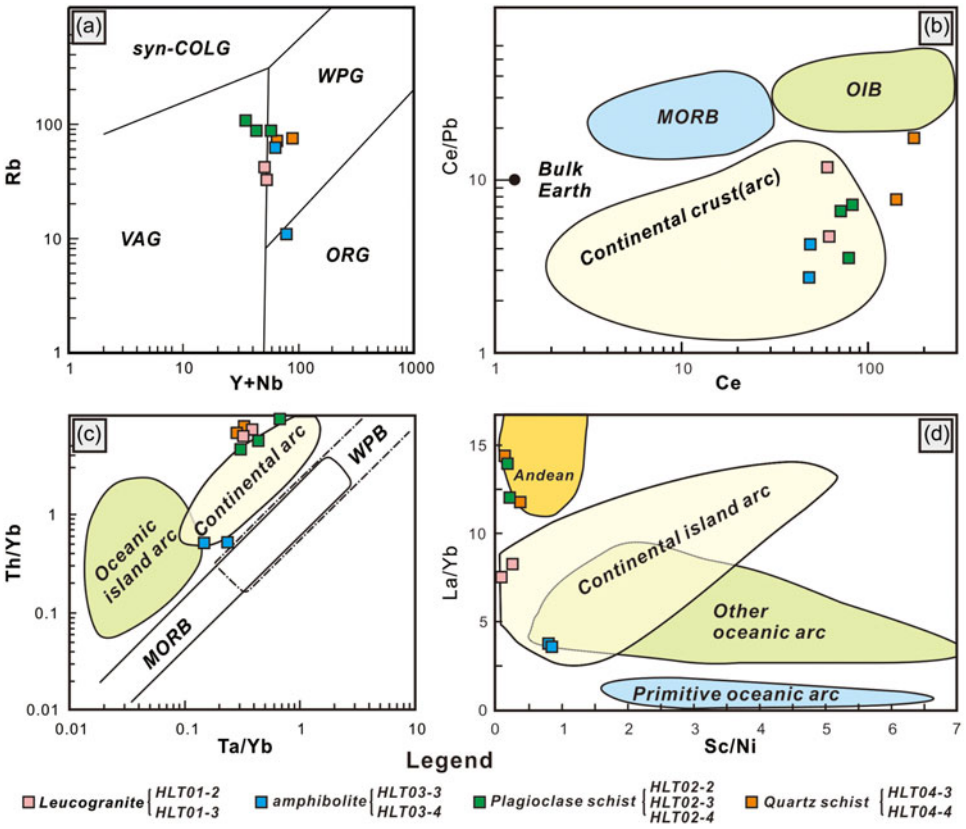

Figure 11. (a) The (Y + Nb) versus Rb diagram (after Pearce et al., 1984), (b) Ce versus Ce/Pb diagram (after Hofmann, 1988), (c) Ta/Yb versus Th/Yb diagram (after Pearce, 1983), and (d) Sc/Ni versus La/Yb diagram (after Bailey, 1981) of the Hongliutan leucogranite and metamorphic rocks. Abbreviations: MORB–middle ocean ridge basalts, OIB–oceanic island basalts, ORG–ocean ridge granites, syn-COLG–syn-collision granites, VAG–volcanic arc granites, WPB–within-plate basalts and WPG–within-plate granites.

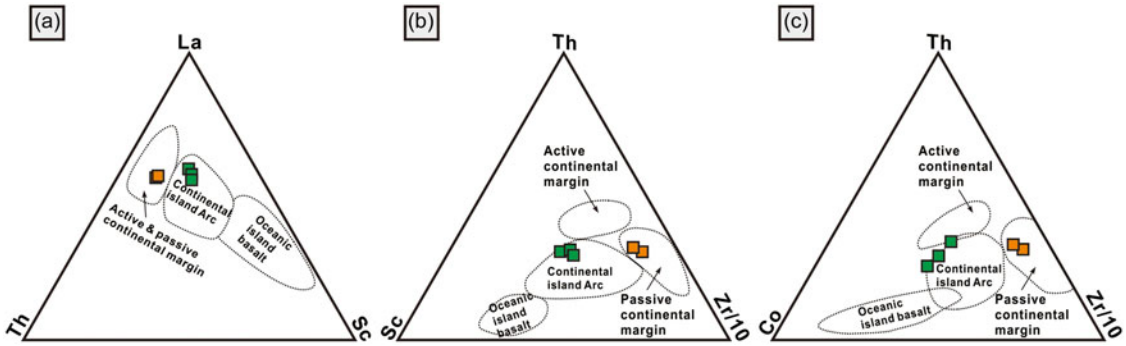

Figure 12. (a) The La-Th-Sc, (b) Th-Sc-Zr/10 and (c) Th-Hf-Co diagrams of the Hongliutan plagioclase schist and quartz schist (after Bhatia and Crook, 1986). Data points for the plagioclase schist (green solid squares) and quartz schist (orange solid squares) are plotted in the continental island arc and passive continental margin fields, respectively.

with oceanic island arcs or ocean ridge settings (Fig. 5e) (e.g. Winter and John 2001; Xu et al., 2015a; Wu et al., 2020; Irvine and Baragar 1971).

(2) There is notable enrichment in Th, U, Zr, and Hf, coupled with the depletion of Nb, Ta, P, and Ti (Fig. 6b; Sun and McDonough, 1989), suggesting a significant crustal component.

(3) The majority of the leucogranite and amphibolite samples are situated at the intersection of within-plate granites and volcanic arc granites on the Y + Nb versus Rb diagram (Fig. 11a; Pearce et al., 1984), and within continental-related crust, arc, or island arc areas on the Ce versus Ce/Pb diagram (Fig. 11b; Hofmann, 1988), the Ta/Yb versus Th/Yb diagram (Fig. 11c; Pearce, 1983), and the Sc/Ni versus La/Yb diagram (Fig. 11d; Bailey, 1981).

(4) The plagioclase schist samples plot within the continental island arc area on the La–Th–Sc (Fig. 12a), Th–Sc–Zr/10 (Fig. 12b), and Th–Hf–Co (Fig. 12c) diagrams (Bhatia and Crook, 1986), while the quartz schist samples are positioned in the passive continental margin field.

(5) High La/Sm ratios, ranging from 5.43 to 6.69, indicate a clear involvement of crustal-derived materials (Lassiter and DePaolo 1997; White 2003).

The U–Pb microanalysis of magmatic zircons in this study has dated the formation of the leucogranite and amphibolite to 506.4 ± 8.0 Ma (Fig. 8b) and 521.8 ± 9.4 Ma (Fig. 9c), respectively. However, their T_{DM}(Nd) ages, ranging from 1.18 to 1.33 Ga and T_{2DM}(Nd) ages from 1.18 to 1.28 Ga, indicate a Mesoproterozoic source of material. These ages are nearly consistent with the 973.7

https://doi.org/10.1017/S0016756824000360

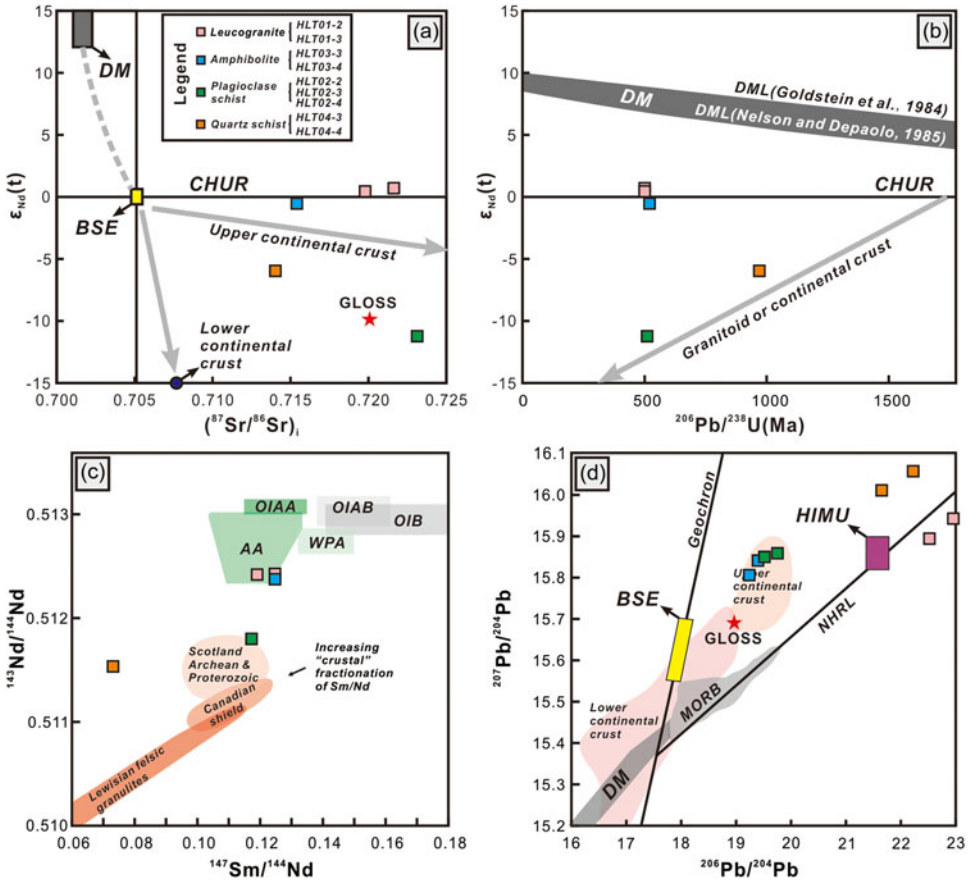

Figure 13. (a) $(^{87}Sr/^{86}Sr)_i$ versus $\varepsilon_{Nd}(t)$ diagram (after Winter and John, 2001; Wu et al., 2003; Tang et al., 2010a, 2010b), (b) $^{206}Pb/^{238}U$(Ma) versus $\varepsilon_{Nd}(t)$ diagram (after Hu et al., 2000; Winter and John, 2001), (c) $^{147}Sm/^{144}Nd$ versus $^{143}Nd/^{144}Nd$ diagram (after Goldstein et al., 1984; Nelson and Depaolo, 1985), and (d) $^{207}Pb/^{204}Pb$ versus $^{206}Pb/^{204}Pb$ diagram (after Hart, 1984; White, 2003; Tang et al., 2010a, 2010b) of the Hongliutan leucogranite and metamorphic rocks. Abbreviations: AA–Andean andesite, BSE–bulk silicate earth, CHUR–chondritic uniform reservoir, DM–depleted mantle, DML–depleted mantle line, Geochron for zero isochron line, GLOSS–global subducting sediment, HIMU–high U/Pb mantle, MORB–mid-ocean ridge basalt, NHRL–north hemisphere reference line, OIAA–oceanic island arc andesite, OIAB–oceanic island arc basalt, OIB–oceanic island basalt, and WPA–within-plate basalt. The data for marine sediments and global subducting sediment (GLOSS) are from Plank and Langmuir (1998) and Chauvel *et al.* (2008).

± 6.2 Ma concordia age of detrital zircons with magmatic characteristics from the quartz schist (Fig. 10c) and the 977.9 ± 28.0 Ma concordia age of inherited zircons within the amphibolite (Fig. 9d). This suggests a significant magmatic-tectonic event during the Neoproterozoic, and it is plausible that this suggests a significant magmatic-tectonic event during the Neoproterozoic, and it is plausible that a Mesoproterozoic basement underlies the area.

The Sr–Nd isotopic compositions of the plagioclase schist and quartz schist, characterized by even older T_{DM}(Nd) ages ranging from 1.74 to 2.12 Ga and T_{2DM}(Nd) ages from 2.12 to 2.14 Ga, along with negative $\varepsilon_{Nd}(t)$ values ranging from −6.0 to −11.3 (Figs. 13a and 13b; Xu et al., 2013, Xu et al., 2015b), indicate the presence of an older basement. This interpretation is further supported by SIMS U–Pb microanalysis, which identified Archaean-Mesoproterozoic inherited zircons in the amphibolite (Fig. 9a; 1566–3064 Ma) and Archaean-Palaeoproterozoic detrital zircons in the quartz schist (Fig. 10a; 1597–3364 Ma). Notably, the concordia age of 2468.1 ± 22.0 Ma for detrital zircons from the quartz schist (Fig. 10d) suggests that the basement may be of Palaeoproterozoic age. These findings support that the Tianshuihai unit is underlain by a Palaeoproterozoic basement that underwent significant tectonic and magmatic reworking during the Neoproterozoic era.

In summary, the metamorphic and igneous rocks within the Hongliutan area were generated in a continental arc setting, indicative of a tectonically active margin. The Tianshuihai unit is underpinned by a Precambrian continental crustal basement, dating back to the Palaeoproterozoic era. It is conceivable that this ancient basement of the Tianshuihai unit underwent significant tectonic reworking during the Neoproterozoic era. However, there is a certain possibility that the aged basement could be an amalgamation of continental crust fragments from various geological periods.

6.c. The petrogenesis of leucogranite and metamorphic rocks

The plagioclase schist exhibits an $\varepsilon_{Nd}(t)$ value of −11.3, a T_{DM}(Nd) age of 2.12 Ga, and a T_{2DM}(Nd) age of 2.14 Ga. In the $(^{87}Sr/^{86}Sr)_i$ versus $\varepsilon_{Nd}(t)$ diagram, it falls between the upper and lower continental crust line (Fig. 13a). In the U–Pb age versus $\varepsilon_{Nd}(t)$ diagram, it is close to the continental crust line (Fig. 13b). It aligns with the Scotland Archaean and Proterozoic field in the $^{147}Sm/^{144}Nd$ versus $^{143}Nd/^{144}Nd$ diagram (Fig. 13c) and falls within the upper continental crust field in the $^{207}Pb/^{204}Pb$ versus $^{206}Pb/^{204}Pb$ diagram (Fig. 13d). The low Sr-Nd isotopic composition and continental crust geochemical affinity (Fig. 10d) suggest that the protolith of plagioclase schist, specifically andesitic tuff, was primarily derived from the anatexis and recycling of intracrustal metaigneous and metasedimentary sources (e.g. Landenberger and Collins, 1996; Jung et al., 2000; Jiang et al., 2005; Jiang et al., 2009; Huang et al., 2011; Wu et al., 2022).

The broad spectrum of $^{207}Pb/^{206}Pb$ ages in the quartz schist ranges from 901 ± 16.8 Ma to 3364 ± 12.8 Ma (Fig. 10a). This is complemented by the $\varepsilon_{Nd}(t)$ value of −6.0, and the T_{DM}(Nd) age of 1.74 Ga, and T_{2DM}(Nd) age of 2.12 Ga. These results collectively suggest a complex provenance for the protolith of the quartz schist, identified as dacitic tuff. It appears to have been formed mainly by the integration of a minor fraction of Neoproterozoic or Mesoproterozoic juvenile materials with more ancient crustal

https://doi.org/10.1017/S0016756824000360

components dating from the Palaeoproterozoic to the Palaeoarchaean.

The amphibolite has an $\varepsilon_{Nd}(t)$ value of −0.6, a $T_{DM}(Nd)$ age of 1.33 Ga, and a $T_{2DM}(Nd)$ age of 1.28 Ga. The U–Pb age versus $\varepsilon_{Nd}(t)$ plot falls between the DM line and continental crust line (Fig. 13b), the $^{147}Sm/^{144}Nd$ versus $^{143}Nd/^{144}Nd$ plot is in the Andean andesite field (Fig. 13c), and the $^{207}Pb/^{204}Pb$ versus $^{206}Pb/^{204}Pb$ plot is in the upper continental crust field (Fig. 13d). These results, combined with a concordia age of 521.8 ± 9.4 Ma for magmatic zircons and inherited zircons ranging from 0.96 to 3.06 Ga (Fig. 9a), suggest that the amphibolite magma was likely derived from Early Cambrian juvenile material, mixed with old Neoproterozoic to Mesoarchaean crust or materials (e.g. Fourcade and Allègre, 1981; Kistler et al., 1986; Lassiter and DePaolo, 1997; Clynne, 1999; White, 2003; Xu et al., 2015a).

The leucogranite has a concordia age of 506.4 ± 8.0 Ma, with $\varepsilon_{Nd}(t)$ value, $T_{DM}(Nd)$ age, and $T_{2DM}(Nd)$ age range from 0.4 to 0.6, 1.18 Ga to 1.45 Ga, and 1.18 Ga to 1.20 Ga. In geochemical diagrams, it aligns with the upper continental crust line in the $(^{87}Sr/^{86}Sr)_i$ versus $\varepsilon_{Nd}(t)$ diagram (Fig. 13a), falls between DM line and continental crust line in the U–Pb age versus $\varepsilon_{Nd}(t)$ diagram (Fig. 13b), and lies in the Andean andesite field in the $^{147}Sm/^{144}Nd$ versus $^{143}Nd/^{144}Nd$ diagram (Fig. 13c). The moderate depletion of Sr-Nd and its continental arc geochemical signature indicate that the leucogranite primarily originated from the mixture of Cambrian juvenile material and old crust or materials (Figs. 10b-d). Considering that amphibolites and leucogranites share similar trace element and isotopic compositions, it is plausible that leucogranites could be formed from the melting of amphibolites. However, there is a lack of additional petrological evidence and direct genetic contact relationships to substantiate this perspective.

6.d. Basement nature of Tashikuergan-Tianshuihai terrane

The nature of the Tashikuergan-Tianshuihai terrane has been subject to debate, with three primary models proposed: (1) a huge accretionary wedge (also known as Tianshuihai accretionary complexes) containing thick flysch sequences between the West Kunlun terrane (also called South Kunlun terrane) and Karakorum terrane, resulting from northward subduction of the Proto-Tethys Ocean from the Cambrian to Triassic periods (Mattern and Schneider, 2000; Wang, 2004; Xiao et al., 2001, 2002, 2003a, 2005; Hu et al., 2017); (2) a section of an arc-like magmatic belt (or a part of the West Kunlun terrane, e.g. Yuan et al., 2003) between the two coexisting Proto-Tethys Oceans (one located between the Karakorum terrane and West Kunlun terrane, and the other between the Tarim and West Kunlun terrane, e.g. Wang et al., 2017). The south- and north-dipping subduction of the Proto-Tethys Ocean beneath the northern and southern margin of the West Kunlun terrane produced this early Palaeozoic arc-like magmatic belt (West Kunlun terrane) (Wang et al., 2017); (3) an independent terrane or microcontinent block (Qiao et al., 2015b; Hu et al., 2016). Zhang et al. (2018a, 2018b, 2019b) proposed that the Proto-Tethys Ocean only existed between the Tarim and southern Kunlun terrane. The Tashikuergan-Tianshuihai terrane on the southern side of the West Kunlun terrane could be considered as a back-arc microcontinent block.

Numerous studies have proposed that the Tashikuergan-Tianshuihai terrane may represent either an accretionary wedge or an arc-like magmatic belt, based on geochemical and isotopic analyses of Palaeozoic-Mesozoic granitoids. These environments are typically characterized by abundant oceanic crust components and pelagic sediments, and igneous rocks predominantly of tholeiitic composition, while synchronously formed volcanic rocks within accretionary wedges are uncommon (Xu et al., 2015a; Wu et al., 2022). However, in this study, all samples analysed belong to the calc-alkaline series and exhibit geochemical characteristics consistent with a continental arc. The presence of terrestrial-derived detrital zircons with limited transportation suggests a more ancient terrane history, contradicting the accretionary wedge or arc models.

Further supporting this interpretation, Ji et al. (2011) documented the presence of inherited zircons dated at 2481 ± 14.0 Ma within Palaeoproterozoic foliated rhyolite in the western part of the Tashikuergan-Tianshuihai terrane. Additional studies have also reported zircon U–Pb ages or bulk rock Rb–Sr ages ranging from 2.13 to 2.77 Ga within the same rock sequence (Pan et al. 2000; Sun et al., 2003; Wang, 2008). In this research, a concordia age of 2468.1 ± 22.0 Ma for detrital zircons from quartz schist was identified in the northeastern part of the Tashikuergan-Tianshuihai terrane. These findings further illuminate the terrane's ancient evolutionary history.

The West Kunlun terrane also has a Palaeoproterozoic basement (ca. 2.5 Ga) composed mainly of gneisses, migmatites, amphibolites, and schists (e.g. Xiao et al., 2003a, 2005; Yuan et al., 2005; Zhang et al., 2018b; Wang et al., 2017; Zhang et al., 2019a; Zhang et al., 2019b; Yin et al., 2020). It is separated from the Tashikuergan-Tianshuihai terrane by the Kangxiwa suture. Similarly, the Tashikuergan-Tianshuihai terrane is separated from the Hoh Xil-Bayan Har block, Qiangtang terrane, and Karakorum terrane by the Dahongliutan fault, Altyn fault, and Qiaoertianshan fault, respectively. These sutures, reactivated by successive faulting, are super-lithospheric faults that delineate distinct tectonic units. Consequently, we suggest that the Tashikuergan-Tianshuihai terrane is a relatively independent terrane with a Precambrian basement. However, the exact relationship, migration, and evolution between the basement of the Tashikuergan-Tianshuihai terrane and that of the West Kunlun terrane remain uncertain.

6.e. The tectonic evolution of Tashikuergan-Tianshuihai terrane

This study identified a NW to SE trend and continuous Palaeoproterozoic basement in the Tashikuergan-Tianshuihai terrane, similar to that located in the adjacent West Kunlun terrane. The Late Archaean-Palaeoproterozoic (ca. 2.7–2.5 Ga) is crucial for granitoid magmatism and the generation of juvenile continental crust in Earth's history (Condie et al., 2009a; Li et al., 2014). According to the age compilation of granitoid rocks, North China, India, and East Antarctica have shown major periods of granitoid production at ca. 2.5 Ga (Condie et al., 2009b; Li et al., 2014). The terrane may also exhibit a geological similarity, such as the Gondwanan affinity observed between Tarim and the North Kunlun terrane of the West Kunlun. Therefore, the c.a. 2.48–2.47 Ga basement in the Tashikuergan-Tianshuihai terrane may be derived from the c.a. 2.5 Ga granitoids in North China, India, and East Antarctica, or from potential underlying Gondwanan crust, indicating that it is a Palaeoproterozoic crustal block.

It is worth noting that the Yangtze Block features tonalite-trondhjemite-granodiorites (TTGs) at ca. 2.1–2.0 Ga, while the rifting-related anorogenic magmatism of the supercontinent Columbia/Nuna in several continents, such as Australia, North

https://doi.org/10.1017/S0016756824000360

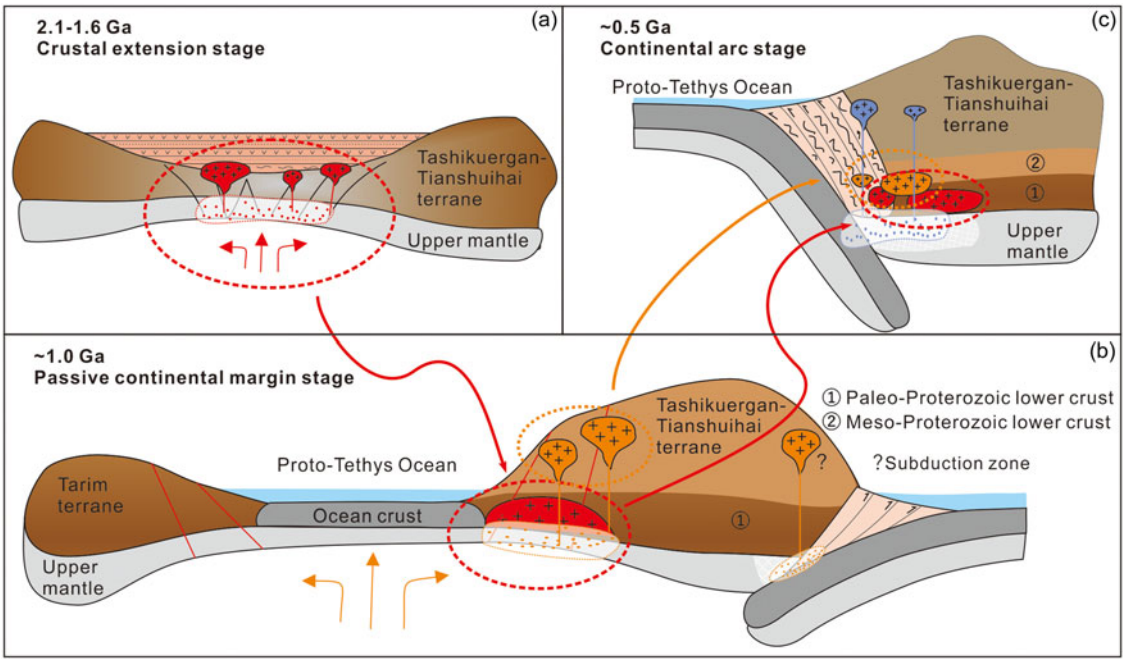

Figure 14. Simplified model illustrating the tectonic evolution of the Tashikuergan-Tianshuihai terrane. (a) The 2.1–1.6 Ga crustal extension stage, (b) the ca. 1.0 Ga passive continental margin stage and (c) the ca. 0.5 Ga continental arc stage. Modified after Zhang et al. (2018c) and Wu et al. (2018).

China, Laurentia, and South America, is centred around ca. 1.8–1.6 Ga (Bickford and Boardman, 1984; Page and Hoatson, 2000; Norcross et al., 2000; Halls et al., 2001; Peng et al., 2008; Li et al., 2014). Therefore, the 2.2–1.6 Ga inherited zircons in amphibolite and the 2.1–1.6 Ga detrital zircons in quartz schist in the Tashikuergan-Tianshuihai terrane may record the break-up of the Columbia/Nuna supercontinent (Fig. 14a). Although the Tashikuergan-Tianshuihai terrane underwent significant transformation and metamorphism due to the tectonic-magmatic activity of the Columbia/Nuna supercontinent, it may also have been amalgamated from younger metasediments (after 2.1–1.6 Ga) that acquired material from a distinct crustal section, not solely from the ancient Tashikuergan-Tianshuihai basement.

The assembly of the supercontinent Rodinia is believed to have taken place around 1.1–0.9 Ga, followed by its disintegration (Li et al., 2008b). The younger Group 1 detrital zircons from the quartz schist, showing magmatic characteristics, display a concordia $^{207}Pb/^{206}Pb$ age of 973.7 ± 6.2 Ma (Fig. 10b). This evidence suggests that the quartz schist protolith formed during the tectonic and magmatic activities related to the Rodinia. This interpretation matches the concordant age of inherited zircons from amphibolite, dated at 977.9 ± 28.0 Ma (Fig. 9d). The geochemical and isotopic signatures reveal that the plagioclase schist and quartz schist are rich in ancient crustal materials. Their protoliths were predominantly derived from the partial melting and recycling of intracrustal metaigneous and metasedimentary rocks, with minor Neoproterozoic or Mesoproterozoic juvenile contributions. They likely formed in a continental arc setting, potentially a rifted (passive) continental margin environment, as shown in Figs. 12a-12d. Subsequent tectonic activities, inducing rifting-related anorogenic magmatism within the Tashikuergan-Tianshuihai terrane, resulted in the formation of plagioclase schist and quartz schist. This event coincided with the initial stages of the Proto-Tethys Ocean's development (Fig. 14b). The formation and disintegration evolution of similar Palaeo-Proterozoic ancient terrane have also been reported in the Wenquan area of West Tianshan, NW China (Central Asian Orogenic Belt, Wang et al., 2014; Liu et al., 2014; Wu et al., 2023).

The magmatic zircons with ages of 506.4 ± 8.0 Ma and 521.8 ± 9.4 Ma from leucogranite and amphibolite, respectively, record Cambrian continental arc-related magmatism, indicating that the Tashikuergan-Tianshuihai terrane experienced the subduction of the Proto-Tethys Ocean (Fig. 14c, Xiao et al., 2002, 2003a, 2005; Li et al., 2007; Hu et al., 2017; Wang et al., 2017; Yin et al., 2020). This magmatism continued until the Silurian and the closing of the Proto-Tethys Ocean (Zhang et al., 2018a). Subsequently, this region entered a new tectonic evolution stage associated with the Palaeo- to Neo-Tethys Ocean (Mattern and Schneider, 2000; Xiao et al., 2005; Jiang et al., 2013; Liu et al., 2015; Yan et al., 2018; Wang et al., 2020).

7. Conclusions

(1) The leucogranite and amphibolite crystallized at 506.4 ± 8.0 Ma and 521.8 ± 9.4 Ma, respectively. The quartz schist is rich in detrital zircons with a broad range of $^{207}Pb/^{206}Pb$ ages extending from 901 to 3364 Ma.

(2) The leucogranite and amphibolite, identified as Cambrian igneous rocks, display distinct geochemical features indicative of a continental arc origin, including calc-alkaline affinity, enrichment in Th, U, Pb, Zr and Hf and depletion in Ba, Nb, Sr and Ti, with $\varepsilon_{Nd}(t)$ values approaching zero.

(3) The younger Group 1 detrital zircons from the quartz schist, exhibiting some magmatic zircon characteristics, have $^{207}Pb/^{206}Pb$ ages ranging from 901 ± 16.8 Ma to 989.9 ± 23.6 Ma, and a concordia age of 973.7 ± 6.2 Ma. This, combined with the 977.9 ± 28.0 Ma concordant age of inherited zircons from the amphibolite, indicates a Neoproterozoic magmatic activity.

https://doi.org/10.1017/S0016756824000360

(4) The plagioclase schist and quartz schist are interpreted as Neoproterozoic volcaniclastic rocks, likely formed in a rifted (passive) continental margin setting.
(5) The U–Pb zircon ages Sr–Nd–Pb isotopic results from quartz schist, amphibolite, leucogranite and metamorphic rocks collectively support the presence of a Palaeoproterozoic basement beneath the Tianshuihai unit that has experienced Neoproterozoic reworking.

Supplementary material. The supplementary material for this article can be found at https://doi.org/10.1017/S0016756824000360.

Data and material availability. All the data are available in Supplementary Table DR 1, 2 and 3.

Acknowledgements. This research was jointly supported by the National Natural Science Foundation of China (Grant Numbers 42302083, 42250202, 41672088 and 42272075) and the Project of Development and Research Center of China Geology Survey (Grant Numbers DD20221785 and DD20230600). We would like to express our gratitude to Dr. Qiang Ke, Dr. Hang Li and Dr. Lei Niu for their invaluable assistance with experimental analyses. Furthermore, the first author would like to extend a heartfelt thank you to his parents and family for their unwavering support and encouragement.

Competing interests. The authors declare that they have no competing interests.

Ethics approval and consent to participate. Not applicable.

Consent for publication. Not applicable.

Reference

Andersen T (2002) Correction of common lead in U–Pb analyses that do not report 204Pb. *Chemical Geology* **192**(1), 59–79.

Anhui Geological Survey (2005a) *Geological Map and Explanatory Text of Wenquan District, China*. Geological Survey Map I44C002001, scale 1:250000. Beijing: Geological Publishing House (in Chinese).

Anhui Geological Survey (2005b) *Geological Map and Explanatory Text of Songxi District, China*. Geological Survey Map I44C002002, scale 1:250000. Beijing: Geological Publishing House (in Chinese).

Bailey JC (1981) Geochemical criteria for a refined tectonic discrimination of orogenic andesites. *Chemical Geology* **32**(1), 139–154.

Bas MJL, Maitre RWL, Streckeisen A, Zanettin B and Iugs (1986) A chemical classification of volcanic rocks based on the total alkali-silica diagram. *Journal of Petrology* **27**(3), 745–750.

Belousova E, Griffin W, O'Reilly SY and Fisher N (2002) Igneous zircon: trace element composition as an indicator of source rock type. *Contributions to Mineralogy and Petrology* **143**(5), 602–622.

Bhatia MR and Crook KAW (1986) Trace element characteristics of graywackes and tectonic setting discrimination of sedimentary basins. *Contributions to Mineralogy and Petrology* **92**(2), 181–193.

Bickford ME and Boardman SJ (1984) A proterozoic volcano-plutonic terrane, Gunnison and Salida Areas, Colorado. *The Journal of Geology* **92**(6), 657–666.

Boynton W (1984) Geochemistry of the rare earth elements: meteorite studies.

Chauvel C, Lewin E, Carpentier M, Arndt NT and Marini JC (2008) Role of recycled oceanic basalt and sediment in generating the Hf–Nd mantle array. *Nature Geoscience* **1**, 64–67.

Chu SX (2008) Preliminary study on regional metallogenic background and metallogenic regularity of West Kunlun and its adjacent area. Unpublished M.Sc. thesis, Beijing, China University of Geosciences, 1–113 (in Chinese).

Chung SL, Chu MF, Zhang Y, Xie Y, Lo CH, Lee TY, Lan CY, Li X, Zhang Q and Wang Y (2005) Tibetan tectonic evolution inferred from spatial and temporal variations in post-collisional magmatism. *Earth-Science Reviews* **68**(3), 173–196.

Clynne MA (1999) A complex magma mixing origin for rocks erupted in 1915, Lassen Peak, California. *Journal of Petrology* **40**(1), 105–132.

Condie KC, Belousova E, Griffin WL and Sircombe KN (2009a) Granitoid events in space and time: Constraints from igneous and detrital zircon age spectra. *Gondwana Research* **15**(3), 228–242.

Condie KC, O'Neill C and Aster RC (2009b) Evidence and implications for a widespread magmatic shutdown for 250 My on Earth. *Earth and Planetary Science Letters* **282**(1), 294–298.

Corfu F, Hanchar JM, Hoskin PWO and Kinny P (2003) Atlas of Zircon Textures. *Reviews in Mineralogy and Geochemistry* **53**(1), 469–500.

Deng WM (1995) Geological features of ophiolite and tectonic significance in the Karakorum West Kunlun Mts. *Acta Petrologica Sinica* **S1**, 98–111 (in Chinese with English abstract).

Ding DG, Wang DX, Liu WX and Sun SQ (1996) *The West Kunlun Orogenic Belts and Basins*. Beijing: Geological Publishing House, 1–143 (in Chinese with English abstract).

Dong LH, Xu XW, Fan TB, Qu X, Li H, Wan JL, An HT, Zhou G, Li JH, Chen G and Liu C (2015) Discovery of the Huoshaoyun super-large exhalative-sedimentary carbonate Pb–Zn deposit in the Western Kunlun Area and its great significance for regional metallogeny. *Xinjiang Geology* **33**, 41–50 (in Chinese with English abstract).

Fourcade S and Allegre CJ (1981) Trace elements behavior in granite genesis: A case study The calc-alkaline plutonic association from the Querigut complex (Pyrénées, France). *Contributions to Mineralogy and Petrology* **76**(2), 177–195.

Goldstein SL, O'Nions RK and Hamilton PJ (1984) A Sm-Nd isotopic study of atmospheric dusts and particulates from major river systems. *Earth and Planetary Science Letters* **70**(2), 221–236.

Halls HC, Campal N, Davis DW and Bossi J (2001) Magnetic studies and U–Pb geochronology of the Uruguayan dyke swarm, Rio de la Plata craton, Uruguay: paleomagnetic and economic implications. *Journal of South American Earth Sciences* **14**(4), 349–361.

Hanchar JM and Rudnick RL (1995) Revealing hidden structures: the application of cathodoluminescence and backscattered electron imaging to dating zircons from lower crustal xenoliths. *Lithos* **36**, 289–303.

Hart SR (1984) A large-scale isotope anomaly in the Southern Hemisphere mantle. *Nature* **309**(5971), 753–757.

Hofmann AW (1988) Chemical differentiation of the Earth: the relationship between mantle, continental crust, and oceanic crust. *Earth and Planetary Science Letters* **90**(3), 297–314.

Hong T, Klemd R, Gao J, Xiang P, Xu X-W, You J, Wang X-S, Wu C, Li H and Ke Q (2017) The tectonic evolution of the Irtysh tectonic belt: New zircon U–Pb ages of arc-related and collisional granitoids in the Kalaxiangar tectonic belt, NW China. *Lithos* **272–273**, 46–68.

Hong T, Xu X-W, Gao J, Peters SG, Zhang D, Jielili R, Xiang P, Li H, Wu C, You J, Liu J and Ke Q (2018) Ore-forming adakitic porphyry produced by fractional crystallization of oxidized basaltic magmas in a subcrustal chamber (Jiamate, East Junggar, NW China). *Lithos* **296–299**, 96–112.

Hu A, Jahn B, Zhang G, Chen Y and Zhang Q (2000) Crustal evolution and Phanerozoic crustal growth in northern Xinjiang: Nd isotopic evidence. Part I. Isotopic characterization of basement rocks. *Tectonophysics* **328**(1), 15–51.

Hu J, Wang H, Huang C, Tong L, Mu S and Qiu Z (2016) Geological characteristics and age of the Dahongliutan Fe-ore deposit in the Western Kunlun orogenic belt, Xinjiang, northwestern China. *Journal of Asian Earth Sciences* **116**, 1–25.

Hu J, Wang H, Mu SL, Wang M and Hou XW (2017) Geochemistry and Hf isotopic compositions of Early Paleozoic granites in Nanpingxueshan from Tianshuihai terrane, West Kunlun: crust-mantle magmatism. *Acta Geologica Sinica* **91**(6), 1192–1207 (in Chinese with English abstract).

Huang H-Q, Li X-H, Li W-X and Li Z-X (2011) Formation of high δ18O fayalite-bearing A-type granite by high-temperature melting of granulitic metasedimentary rocks, southern China. *Geology* **39**(10), 903–906.

Irvine TN and Baragar WRA (1971) A guide to the chemical classification of the common volcanic rocks. *Canadian Journal of Earth Sciences* **8**(5), 523–548.

Ji WH, Li RS, Chen SJ, He SP, Zhao ZM, Bian XW, Zhu HP, Cui JG and Ren JG (2011) The discovery of Palaeoproterozoic volcanic rocks in the Bulunkuoler Group from the Tianshuihai Massif in Xinjiang of Northwest China and its geological significance. *Science China-earth Sciences* **54**, 61–72 (in Chinese). https://doi.org/10.1007/s11430-010-4043-7.

Jia RY, Jiang YH, Liu Z, Zhao P and Zhou Q (2013) Petrogenesis and tectonic implications of early Silurian high-K calc-alkaline granites and their potassic microgranular enclaves, western Kunlun orogen, NW Tibetan Plateau. *International Geology Review*.

Jiang C, Yang JS, Feng BG, Zhu ZZ, Zhao M, Chai YC, Shi XD, Wang HD and Hu JQ (1992) *Opening-closing tectonics of Kunlun Mountains, Geological Memoirs, Series 5, Number 12*, Beijing: Geological Publishing House, 1–224 (in Chinese with English abstract).

Jiang N, Zhang S, Zhou W and Liu Y (2009) Origin of a Mesozoic granite with A-type characteristics from the North China craton: highly fractionated from I-type magmas? *Contributions to Mineralogy and Petrology* **158**(1), 113–130.

Jiang YH, Jia RY, Liu Z, Liao SY, Zhao P and Zhou Q (2013) Origin of Middle Triassic high-K calc-alkaline granitoids and their potassic microgranular enclaves from the western Kunlun orogen, northwest China: A record of the closure of Paleo-Tethys. *Lithos* **156–159**, 13–30.

Jiang YH, Jiang SY, Ling HF, Zhou XR, Rui XJ and Yang WZ (2002) Petrology and geochemistry of shoshonitic plutons from the western Kunlun orogenic belt, Xinjiang, northwestern China: implications for granitoid geneses. *Lithos* **63**(3), 165–187.

Jiang YH, Ling HF, Jiang SY, Fan HH, Shen WZ and Ni P (2005) Petrogenesis of a Late Jurassic Peraluminous volcanic complex and its High-Mg, Potassic, Quenched Enclaves at Xiangshan, Southeast China. *Journal of Petrology* **46**(6), 1121–1154.

Jung S, Hoernes S and Mezger K (2000) Geochronology and petrogenesis of Pan-African, syn-tectonic, S-type and post-tectonic A-type granite (Namibia): products of melting of crustal sources, fractional crystallization and wall rock entrainment. *Lithos* **50**(4), 259–287.

Kistler RW, Chappell BW, Peck DL and Bateman PC (1986) Isotopic variation in the Tuolumne Intrusive Suite, central Sierra Nevada, California. *Contributions to Mineralogy and Petrology* **94**(2), 205–220.

Landenberger B and Collins WJ (1996) Derivation of A-type granites from a dehydrated charnockitic lower crust: evidence from the Chaelundi Complex, Eastern Australia. *Journal of Petrology* **37**(1), 145–170.

Lassiter JC and DePaolo DJ (1997) Plume/Lithosphere Interaction in the Generation of Continental and Oceanic Flood Basalts: Chemical and Isotopic Constraints. In *Large Igneous Provinces: Continental, Oceanic, and Planetary Flood Volcanism*, pp. 335–355. American Geophysical Union (AGU).

Li CF, Chu ZY, Guo JH, Li YL, Yang YH and Li XH (2015) A rapid single column separation scheme for high-precision Sr–Nd–Pb isotopic analysis in geological samples using thermal ionization mass spectrometry. *Analytical Methods* **7**(11), 4793–4802.

Li CF, Wang XC, Guo JH, Chu ZY and Feng LJ (2016) Rapid separation scheme of Sr, Nd, Pb, and Hf from a single rock digest using a tandem chromatography column prior to isotope ratio measurements by mass spectrometry. *Journal of Analytical Atomic Spectrometry* **31**(5), 1150–1159.

Li H, Xu XW, Borg G, Albert Gilg H, Dong LH, Fan TB, Zhou G, Liu R-L, Hong T, Ke Q, Wu C, Zhang G and Li H (2019) Geology and geochemistry of the giant Huoshaoyun zinc-lead deposit, Karakorum Range, northwestern Tibet. *Ore Geology Reviews* **106**, 251–272.

Li RS, Ji WH, Yang YC, Pan XP, Yu PS, Chen SJ, Zhao ZM, Yang JL, Meng Y, Luo CY, Li X and Zhang WJ (2009a) *1:1000000 Geological Map of Kunlun Mountains and Its Adjacent Region*. Beijing, Geological Publishing House (in Chinese).

Li RS, Ji WH, Yang YC, Yu PS, Zhao ZM, Chen SJ, Meng Y, Pan XP, Shi BD, Zhang WJ, Li X and Luo CY (2008a) *Geology of Kunlun Mountains and Its Adjacent Region*. Beijing, Geological Publishing House, 384–388 (in Chinese).

Li RS, Ji WH, Zhao ZM, Chen SJ, Meng Y, Yu PS and Pan XP (2007) Progress in the study of the Early Paleozoic Kunlun orogenic belt. *Geological Bulletin of China* **26**(4), 373–382 (in Chinese).

Li XH, Li ZX and Li WX (2014) Detrital zircon U–Pb age and Hf isotope constrains on the generation and reworking of Precambrian continental crust in the Cathaysia Block, South China: A synthesis. *Gondwana Research* **25**(3), 1202–1215.

Li XH, Liu Y, Li QL, Guo C-H and Chamberlain KR (2009b) Precise determination of Phanerozoic zircon Pb/Pb age by multicollector SIMS without external standardization. *Geochemistry, Geophysics, Geosystems* **10**(4).

Li ZX, Bogdanova SV, Collins AS, Davidson A, De Waele B, Ernst RE, Fitzsimons ICW, Fuck RA, Gladkochub DP, Jacobs J, Karlstrom KE, Lu S, Natapov LM, Pease V, Pisarevsky SA, Thrane K and Vernikovsky V (2008b) Assembly, configuration, and break-up history of Rodinia: A synthesis. *Precambrian Research* **160**(1), 179–210.

Liu H, Wang B, Shu L, Jahn B and Lizuka Y (2014) Detrital zircon ages of Proterozoic meta-sedimentary rocks and Paleozoic sedimentary cover of the northern Yili Block: Implications for the tectonics of microcontinents in the Central Asian Orogenic Belt. *Precambrian Research* **252**, 209–222.

Liu XF (1991) *Laboratory Research Methods of Sedimentary Rocks*. Beijing: Geology Press, 213–218.

Liu Z, Jiang Y-H, Jia R-Y, Zhao P and Zhou Q (2015) Origin of Late Triassic high-K calc-alkaline granitoids and their potassic microgranular enclaves from the western Tibet Plateau, northwest China: Implications for Paleo-Tethys evolution. *Gondwana Research* **27**(1), 326–341.

Long X, Sun M, Yuan C, Xiao W, Lin S, Wu F, Xia X and Cai K (2007) Detrital zircon age and Hf isotopic studies for metasedimentary rocks from the Chinese Altai: Implications for the Early Paleozoic tectonic evolution of the Central Asian Orogenic Belt. *Tectonics* **26**(5).

Ludwig KR (2001) *SQUID 1.02: A User's Manual*. Berkeley Geochronology Center, *Special Publication* **2**, 1–19.

Maniar PD and Piccoli PM (1989) Tectonic discrimination of granitoids. *GSA Bulletin* **101**(5), 635–643.

Matte Ph, Tapponnier P, Arnaud N, Bourjot L, Avouac JP, Vidal Ph, Qing L, Yusheng P and Yi W (1996) Tectonics of Western Tibet, between the Tarim and the Indus. *Earth and Planetary Science Letters* **142**(3), 311–330.

Mattern F and Schneider W (2000) Suturing of the Proto- and Paleo-Tethys oceans in the western Kunlun (Xinjiang, China). *Journal of Asian Earth Sciences* **18**(6), 637–650.

Nelson BK and Depaolo DJ (1985) Rapid production of continental crust 1.7 to 1.9 b.y. ago: Nd isotopic evidence from the basement of the North American mid-continent. *GSA Bulletin* **96**(6), 746–754.

Norcross C, Davis DW, Spooner ETC and Rust A (2000) U–Pb and Pb–Pb age constraints on Paleoproterozoic magmatism, deformation and gold mineralization in the Omai area, Guyana Shield. *Precambrian Research* **102**(1), 69–86.

Page RW and Hoatson DM (2000) Geochronology of mafic-ultramafic intrusions. *Australian Geological Survey Organization Bulletin* **246**, 163–172.

Pan G, Wang L, Li R, Yuan S, Ji W, Yin F, Zhang W and Wang B (2012) Tectonic evolution of the Qinghai-Tibet Plateau. *Journal of Asian Earth Sciences* **53**, 3–14.

Pan GT, Zhu DC, Wang LQ, Liao ZL, Geng QR and Jiang XS (2004) Banggong Lake-Nu River suture zone-the northern boundary of Gondwanaland: evidence from geology and geophysics. *Earth Science Frontiers* **11**(4), 371–382 (in Chinese with English abstract).

Pan YS (1990) Tectonic features and evolution of the western Kunlun Mountain Region. *Scientia Geologica Sinica* **25**, 224–232 (in Chinese with English abstract).

Pan YS (1996). Geological evolution of Karakorum and Kunlun Mountains. In: Pan, Y.S. (Ed.), *Regional Geological Evolution and Conclusion*. Beijing: Seismological Press, 263–288 (in Chinese).

Pan YS, Wen SX, Sun DL, *et al* (2000) *Geological Evolution of the Karakornm-Kunlun Mountains*. Beijing, Science Press, 1–525 (in Chinese).

Pearce J (1983) Role of the sub-continental lithosphere in magma genesis at active continental margin. *Continental Basalts and Mantle Xenoliths*, 230–249.

Pearce JA, Harris NBW and Tindle AG (1984) Trace element discrimination diagrams for the tectonic interpretation of granitic rocks. *Journal of Petrology* **25**(4), 956–983.

Peng P, Zhai M, Ernst RE, Guo J, Liu F and Hu B (2008) A 1.78 Ga large igneous province in the North China craton: The Xiong'er Volcanic Province and the North China dyke swarm. *Lithos* **101**(3), 260–280.

Pietranik AB, Hawkesworth CJ, Storey CD, Kemp AIS, Sircombe KN, Whitehouse MJ and Bleeker W (2008) Episodic, mafic crust formation from

https://doi.org/10.1017/S0016756824000360

4.5 to 2.8 Ga: New evidence from detrital zircons, Slave craton, Canada. *Geology* **36**(11), 875–878.

Plank T and Langmuir CH (1998) The chemical composition of subducting sediment and its consequences for the crust and mantle. *Chemical Geology* **145**, 325–394.

Qiao GB, Wang P, Wu YZ, Hao YH, Zhao XJ, Chen DH, Lv PR and Du W (2015b) Formation age of ore bearing strata of the Zankan iron deposit in Taxkorgan landmass of western Kunlun Mountains and its geological significance. *Geology in China* **42**, 616–630 (in Chinese with English abstract).

Qiao GB, Zhang HD, Wu YZ, Jin MS, Du W, Zhao XJ and Chen DH (2015a) Petrogenesis of the Dahongliutan monzogranite in western Kunlun: constraints from SHRIMP zircon U–Pb geochronology and geochemical characteristics. *Acta Geologica Sinica* **89**, 1180–1194 (in Chinese with English abstract).

Rojas-Agramonte Y, Kröner A, Demoux A, Xia X, Wang W, Donskaya T, Liu D and Sun M (2011) Detrital and xenocrystic zircon ages from Neoproterozoic to Palaeozoic arc terranes of Mongolia: Significance for the origin of crustal fragments in the Central Asian Orogenic Belt. *Gondwana Research* **19**(3), 751–763.

Shen WZ, Shu LS, Xiang L, Zhang FR and Wang B (2009) Geochemical characteristics of Early Paleozoic sedimentary rocks in the Jinggangshan area, Jiangxi province and the constraining to the sedimentary environment. *Acta Petrologica Sinica* **25**, 2442–2458.

Sun and **McDonough W** (1989) Chemical and isotopic systematics of oceanic basalts: Implications for mantle composition and processes. In *Geological Society, London, Special Publications*.

Sun HT, Li CJ, Wu H, Wang HJ, Qi SJ, Chen GM, Liu ZT and Gao P (2003) *Introduction to West Kunlun Metallogenic Province*. Beijing: Geological Publishing House, 1–255 (in Chinese).

Tang G, Wang Q, Wyman DA, Li ZX, Zhao ZH, Jia XH and Jiang ZQ (2010a) Ridge subduction and crustal growth in the Central Asian Orogenic Belt: Evidence from Late Carboniferous adakites and high-Mg diorites in the western Junggar region, northern Xinjiang (west China). *Chemical Geology* **277**(3), 281–300.

Tang GJ, Wang Q, Wyman DA, Sun M, Li ZX, Zhao ZH, Sun WD, Jia XH and Jiang ZQ (2010b) Geochronology and geochemistry of Late Paleozoic magmatic rocks in the Lamasu–Dabate area, northwestern Tianshan (west China): Evidence for a tectonic transition from arc to post-collisional setting. *Lithos* **119**(3), 393–411.

Wang B, Liu H, Shu L, Jahn B, Chung S, Zhai Y and Liu D (2014) Early Neoproterozoic crustal evolution in northern Yili Block: Insights from migmatite, orthogneiss and leucogranite of the Wenquan metamorphic complex in the NW Chinese Tianshan. *Precambrian Research* **242**, 58–81.

Wang C, Liu L, Korhonen F, Yang WQ, Cao YT, He SP, Zhu XH and Liang WT (2016) Origins of Early Mesozoic granitoids and their enclaves from West Kunlun, NW China: implications for evolving magmatism related to closure of the Paleo-Tethys Ocean. *International Journal of Earth Sciences* **105**(3), 941–964.

Wang H, Gao H, Wang SM, Yan QH, Wang ZH, Huang L and Qin Y (2022) Zircon and columbite-tantalite U–Pb geochronology of Li–Be rare metal pegmatite and its geological significance in Muji area, West Kunlun, China. *Acta Petrologica Sinica* **38**(7), 1937–1951. https://doi.org/10.18654/1000-0569/2022.07.08.

Wang H, Gao H, Zhang XY, Yan QH, Xu Y, Zhou K, Dong R and Li P (2020) Geology and geochronology of the super-large Bailongshan Li–Rb–(Be) rare-metal pegmatite deposit, West Kunlun orogenic belt, NW China. *Lithos* **360–361**, 105449.

Wang J, Hattori K, Liu J, Song Y, Gao Y and Zhang H (2017) Shoshonitic- and adakitic magmatism of the Early Paleozoic age in the Western Kunlun orogenic belt, NW China: Implications for the early evolution of the northwestern Tibetan plateau. *Lithos* **286–287**, 345–362.

Wang JP (2008) Geological features and tectonic significance of mélange zone in the Taxkorgan area, West Kunlun. *Geological Bulletin of China* **27**(12), 2057–2066 (in Chinese with English abstract).

Wang W (2004) Tectonic evolution of the western Kunlun orogenic belt, western China. *Journal of Asian Earth Sciences* **24**(2), 153–161.

Wei XP, Wang H, Hu J, Mu SL, Qiu ZW, Yan QH and Li P (2017) Geochemistry and geochronology of the Dahongliutan two-mica granite pluton in western Kunlun orogeny. *Geochimica* **1** 66–80 (in Chinese with English abstract).

White WM (2003) *Geochemistry*. John-Hopkins University Press, 1–701.

Wilson M ed. (1989f) *Igneous Petrogenesis*, Dordrecht: Springer Netherlands.

Winchester JA and Floyd PA (1977) Geochemical discrimination of different magma series their differentiation products using immobile elements. *Chemical Geology* **20**, 325–343. https://doi.org/10.1016/0009-2541(77)90057-2.

Winter JD and John D (2001) *An Introduction to Igneous and Metamorphic Petrology*, Upper Saddle River, NJ: Prentice Hall, 730 p.

Wu C, Hong T, Xu X, Wang C and Dong L (2023) Report of 2.7 Ga zircon U–Pb age of orthogneiss in the Wenquan metamorphic complex, West Tianshan, China. *China Geology* **6**(1), 168–170.

Wu C, Hong T, Xu XW, Cao MJ, Li H, Zhang GL, You J, Ke Q and Dong LH (2018) Tectonic evolution of the Paleozoic Barluk continental arc, West Junggar, NW China. *Journal of Asian Earth Sciences* **160**, 48–66.

Wu C, Hong T, Xu XW, Li H, Ke Q, Li H and Dong LH (2020) Constraints on the nature of the basement of the Junggar terrane indicated by the Laba Ordovician continental arc. *International Geology Review* **62**(1), 29–52.

Wu C, Hong T, Xu XW, Wang CX and Dong LH (2022) A-type granites induced by a breaking-off and delamination of the subducted Junggar oceanic plate, West Junggar, Northwest China. *China Geology* **5**(3), 457–474.

Wu F, Jahn B, Wilde SA, Lo C-H, Yui TF, Lin Q, Ge W and Sun D (2003) Highly fractionated I-type granites in NE China (II): isotopic geochemistry and implications for crustal growth in the Phanerozoic. *Lithos* **67**(3), 191–204.

Xiao W, Han F, Windley BF, Yuan C, Zhou H and Li J (2003a) Multiple accretionary orogenesis and episodic growth of continents: Insights from the Western Kunlun Range, Central Asia. *International Geology Review*.

Xiao W, Windley BF, Hao J and Zhai M. (2003b) Accretion leading to collision and the Permian Solonker suture, Inner Mongolia, China: Termination of the central Asian orogenic belt. *Tectonics* **22**(6). https://doi.org/10.1029/2002TC001484.

Xiao WJ, Windley BF, Chen HL, Zhang GC and Li JL (2002) Carboniferous-Triassic subduction and accretion in the western Kunlun, China: Implications for the collisional and accretionary tectonics of the northern Tibetan Plateau. *Geology* **30**(4), 295–298.

Xiao WJ, Windley BF, Fang AM, Zhou H, Yuan C, Wang ZH, Hao J, Hou QL and Li JL (2001) Palaeozoic-Early Mesozoic Accretionary Tectonics of the Western Kunlun Range, NW China. *Gondwana Research* **4**(4), 826–827.

Xiao WJ, Windley BF, Liu DY, Jian P, Liu CZ, Yuan C and Sun M (2005) Accretionary tectonics of the Western Kunlun Orogen, China: A Paleozoic–Early Mesozoic, long-lived active continental margin with implications for the growth of Southern Eurasia. *The Journal of Geology* **113**(6), 687–705.

Xie L, Zhang Y, Zhang H, Sun J and Wu F (2008) In situ simultaneous determination of trace elements, U–Pb and Lu–Hf isotopes in zircon and baddeleyite. *Chinese Science Bulletin* **53**(10), 1565–1573.

Xu XW, Jiang N, Li XH, Qu X, Yang YH, Mao Q, Wu Q, Zhang Y and Dong LH (2013) Tectonic evolution of the East Junggar terrane: Evidence from the Taheir tectonic window, Xinjiang, China. *Gondwana Research* **24**(2), 578–600.

Xu XW, Jiang N, Li XH, Wu C, Qu X, Zhou G and Dong LH (2015b) Spatial–temporal framework for the closure of the Junggar Ocean in central Asia: New SIMS zircon U–Pb ages of the ophiolitic mélange and collisional igneous rocks in the Zhifang area, East Junggar. *Journal of Asian Earth Sciences* **111**, 470–491.

Xu XW, Li XH, Jiang N, Li QL, Qu X, Yang YH, Zhou G and Dong LH (2015a) Basement nature and origin of the Junggar terrane: New zircon U–Pb–Hf isotope evidence from Paleozoic rocks and their enclaves. *Gondwana Research* **28**(1), 288–310.

Yan QH, Qiu ZW, Wang H, Wang M, Wei XP, Li P, Zhang RQ, Li CY and Liu J (2018) Age of the Dahongliutan rare metal pegmatite deposit, West Kunlun, Xinjiang (NW China): Constraints from LA–ICP–MS U–Pb dating of columbite-(Fe) and cassiterite. *Ore Geology Reviews* **100**, 561–573.

Yin A and Harrison TM (2000) Geologic Evolution of the Himalayan-Tibetan Orogen. *Annual Review of Earth and Planetary Sciences* **28**, 211–280.

Yin J, Xiao W, Sun M, Chen W, Yuan C, Zhang Y, Wang T, Du Q, Wang X and Xia X (2020) Petrogenesis of Early Cambrian granitoids in the western Kunlun orogenic belt, Northwest Tibet: Insight into early-stage subduction of the Proto-Tethys Ocean. *GSA Bulletin* **132**(9–10), 2221–2240.

Yuan C, Sun M, Zhou M, Zhou H, Xiao W and Li J (2002) Tectonic Evolution of the West Kunlun: Geochronologic and Geochemical Constraints from Kudi Granitoids. *International Geology Review*.

Yuan C, Sun M, Zhou MF, Xiao W and Zhou H (2005) Geochemistry and petrogenesis of the Yishak Volcanic Sequence, Kudi ophiolite, West Kunlun (NW China): implications for the magmatic evolution in a subduction zone environment. *Contributions to Mineralogy and Petrology* **150**(2), 195–211.

Yuan C, Sun M, Zhou MF, Zhou H, Xiao W and Li J (2003) Absence of Archean basement in the South Kunlun Block: Nd–Sr–O isotopic evidence from granitoids. *Island Arc* **12**, 13–21.

Zhang CL, Zou HB, Ye XT and Chen XY (2018a) Tectonic evolution of the NE section of the Pamir Plateau: New evidence from field observations and zircon U–Pb geochronology. *Tectonophysics* **723**, 27–40.

Zhang CL, Zou HB, Ye XT and Chen XY (2018b) Timing of subduction initiation in the Proto-Tethys Ocean: Evidence from the Cambrian gabbros from the NE Pamir Plateau. *Lithos* **314–315**, 40–51.

Zhang CL, Zou HB, Ye XT and Chen XY (2018c) Tectonic evolution of the West Kunlun Orogenic Belt along the northern margin of the Tibetan Plateau: Implications for the assembly of the Tarim terrane to Gondwana. *Geoscience Frontiers* **10**(3), 973–988. https://doi.org/10.1016/j.gsf.2018.05.006.

Zhang CL, Zou HB, Ye XT and Chen XY (2019a) Tectonic evolution of the West Kunlun Orogenic Belt along the northern margin of the Tibetan Plateau: Implications for the assembly of the Tarim terrane to Gondwana. *Geoscience Frontiers* **10**(3), 973–988.

Zhang HS, Ji WH, Ma ZP, Gao XF, Sun C, Hong J and Lv PR (2020) Geochronology and geochemical study of the Cambrian andesite in Tianshuihai Terrane: Implications for the evolution of the Proto-Tethys Ocean in the West Kunlun-Karakoram·Orogenic Belt. *Acta Petrologica Sinica* **36**(1), 257–278 (in Chinese with English abstract). https://doi.org/10.18654/1000-0569/2020.01.21.

Zhang Q, Liu Y, Huang H, Wu Z and Zhou Q (2016) Petrogenesis and tectonic implications of the high-K Alamas calc-alkaline granitoids at the northwestern margin of the Tibetan Plateau: Geochemical and Sr–Nd–Hf–O isotope constraints. *Journal of Asian Earth Sciences* **127**, 137–151.

Zhang Q, Liu Y, Wu Z, Huang H, Li K and Zhou Q (2019b) Late Triassic granites from the northwestern margin of the Tibetan Plateau, the Dahongliutan example: petrogenesis and tectonic implications for the evolution of the Kangxiwa Palaeo-Tethys. *International Geology Review* **61**(2), 175–194.